The Pennsylvania State University

The Graduate School

MICROGRAVITY'S INFLUENCE ON THE HYDRATION OF TRICALCIUM ALUMINATE AND GYPSUM PASTES

A Thesis in

Civil Engineering

by

Peter J. Collins

© 2019 Peter J. Collins

Submitted in Partial Fulfillment
of the Requirements
for the Degree of

Master of Science

December 2019

The thesis of Peter J. Collins was reviewed and approved* by the following:

Aleksandra Radlińska
Associate Professor of Civil and Environmental Engineering
Thesis Advisor

Farshad Rajabipour
Associate Professor of Civil and Environmental Engineering

Barry Scheetz
Professor of Materials, Civil, and Nuclear Engineering

Sven Bilén
Professor of Engineering Design, Electrical Engineering, and Aerospace Engineering
Head of School of Engineering Design, Technology, and Professional Programs

Richard Grugel
Material Scientist – NASA, Marshall Space Flight Center - EM31

Patrick Fox
Shaw Professor of Civil and Environmental Engineering
Department Head of Civil and Environmental Engineering

*Signatures are on file in the Graduate School

ABSTRACT

The hydration of cement is well known to be a complex, multiphase process that continuously transpires. A variable that has not been discussed in depth to date is the influence of gravity on the kinetics of the hydration process. It is envisioned that humans will embark on space exploration missions for extended periods of times which leads to the need of resilient habitats and other pieces of infrastructure. Specifically, as part of the Artemis program, a sustained human presence on the Moon is set for 2028 and it is likely that a cement-like binder from in-situ materials will be used for space habitats. Consequently, the kinetics of cement hydration in extraterrestrial context needs to be better understood as it will likely be different than on Earth. As a first step, various samples were sent to the International Space Station to mix and hydrate in the microgravity environment (10^{-6} g relative to Earth's gravity).

The lack of gravity minimizes transport phenomena due to gravity such as fluid convection and buoyancy. Consequently, this leads to a diffusion-controlled hydration process. At early ages, this promotes enhanced concentration of the reaction products about the decomposing phases. This phenomenon is evident when tricalcium aluminate (C_3A) and gypsum samples hydrated in microgravity are compared to an otherwise identical Earth-based samples. In microgravity, the gypsum experiences morphological differences during dissolution and ettringite is seen to grow on the gypsum along with adjacent pockets of monosulfate.

C_3A and gypsum make up a minor part of portland cements but play a substantial role in the early age kinetics. The addition of gypsum to portland cements hinders the rapid reaction of the C_3A with water, effectively negating a flash set. Gypsums phenomenon in hindering the reaction of C_3A is what allows for concrete to be mixed, transported, placed, and finished before setting on Earth. Such phenomenon needs to be understood as a function of gravity in order to lead toward effective mixture designs for a cement-like binder using in-situ planetary materials.

Here it is noted that the amount of gypsum within the mixture plays a substantial role in the microstructural development in microgravity as compared to a terrestrial gravity sample.

TABLE OF CONTENTS

LIST OF FIGURES vii

LIST OF TABLES x

ACKNOWLEDGEMENTS xi

Chapter 1 Project Background and Objectives 1

1.1 Project Introduction 1
1.2 Research Objectives 2
1.3 Thesis Outline 4

Chapter 2 Literature Review 6

2.1 Reactions Associated with C_3A and Gypsum 6
2.2 Gypsum Dissolution and Phenomena within C_3A 8
2.3 Published Cement Microgravity Solidification Projects 16

Chapter 3 Materials and Characterization Methods 18

3.1 Pouch Design and Mixing Procedure 18
3.2 Materials and Sample Design 20
3.3 Scanning Electron Microscopy (SEM) 21
3.3.1 Image Analysis 22
3.4 X-Ray Diffraction (XRD) 25

Chapter 4 Results and Discussion 27

4.1 Series 1 Results and Discussion 27
4.1.1 Microstructural Differences at 2.18 and 2.58 Hours 28
4.1.2 Microstructural Differences at 6.23 Hours 34
4.1.3 Microstructural Differences at 22.97 Hours 35
4.1.4 Microstructural Differences for the Non-Flushed Specimen 36
4.1.5 Porosity Analysis for Series 1 37
4.2 Series 2 Results and Discussion 38
4.2.1 Microstructural Differences at 2.47 Hours. 38
4.2.2 Microstructural Differences at 6.10 Hours 44
4.2.3 Microstructural Differences at 23.35 Hours 46
4.2.4 Microstructural Differences for the Non-Flushed Specimen 49

Chapter 5 Conclusions and Future Work 50

5.1 Summary of Findings 50
5.2 Future Work 51

Appendix A Supplemental Studies 53

A.1 Clinostat Study 53
A.2 Prolonged Alcohol Exposure Study 57

References 59

LIST OF FIGURES

Figure 2-1 – A schematic showing the basic AFm structure (Baquerizo, Matschei, & Scrivener, 2016). 7

Figure 2-2 – An image from Fan and Teng showing the molecular structure of gypsum and how the etch pits form on the two surfaces (Fan & Teng, 2007). The calcium, sulfur, oxygen, and hydrogen are represented by the large black circles, small black circles, half colored circles, and small white circles, respectively. 10

Figure 2-3 – An AFM image showing the etch pits that form with respect to the [1 0 0] and [0 0 1] direction (Zareeipolgardani et al., 2017). 11

Figure 2-4 – An image from the published MICS C_3S paper showing the difference in porosity, C-S-H, and CH (Moraes Neves et al., 2019)..... 17

Figure 3-1 – Astronaut Alexander Gerst is mixing one of the MICS samples within the glovebox on the Maintenance Work Bench on the ISS (NASA, 2018). 18

Figure 3-2 – On the left is an example of a three-compartment pouch that has been mixed, clipped, and flushed with alcohol. On the right is a two-compartment pouch that has been mixed and clipped. After the samples were mixed they were placed in the sealable bag also seen in the right image. 19

Figure 3-3 – The particle size distribution of the C_3A and gypsum used within the study..... 20

Figure 3-4 – The process for thresholding an image is shown starting at the original image. The typical greyscale histogram in the top right is converted into a cumulative curve in order to apply the overflow method. The original histogram shows a slight shoulder on the right side of the major hump, which would be the characteristic location of the C_3AH_6. The two linear lines are drawn until their intersection which leads to the greyscale value of 40 used to produce the final binary image for calculating the area of porosity. 25

Figure 3-5 – A prepared XRD sample within the airtight dome sample holder. 26

Figure 4-1 – The XRD patterns for the Series 1 samples alternating terrestrial gravity and microgravity with the age of hydration increasing from the bottom to top. The letters marking the main peaks represent (A) C_3A, (B) gypsum, (C) ettringite, (D) m-AFm, (E) hemicarboaluminate, (F) hydrogarnet, and (G) hydroxy-AFm (C_4AH_{19}). 28

Figure 4-2 – a) Shows a piece of gypsum from the terrestrial sample after 2 hours and 11 minutes of hydration. It has a smooth surface with minimal striations. b) Shows two pieces of gypsum from the microgravity sample at the same 2 hour and 11 minute time. The gypsum in the microgravity sample is heavily striated and the top piece has growth of ettringite. c) Dense ettringite growth with very little gypsum remaining. d) A cloud of hydration products shows the past site of an original piece of gypsum. 30

Figure 4-3 – On the left is a slightly striated gypsum crystal from 2 hours and 35 minutes of hydration on Earth. At the same hydration time, the gypsum in the microgravity sample is heavily striated with substantial ettringite growth on it and showing the AFm clusters nearby. 32

Figure 4-4 – A large area of AFm plates that likely used to be the place of a piece of gypsum. 32

Figure 4-5 – On the left is the polished cross-section of the terrestrial sample that hydrated for 2 hours and 35 minutes and on the right is the microgravity sample at an identical time. The micogravity sample lacks a uniform distribution of hydration products. 33

Figure 4-6 – The terrestrial gravity and microgravity sample on the left and right, respectively, show a significant difference in the amount of trapped air within the matrix. 34

Figure 4-7 – Two images with a magnification of 500× for the samples that hydrated for 6 hours and 14 minutes, with terrestrial gravity being on the left and microgravity on the right. 35

Figure 4-8 – A comparison of the polished samples for the terrestrial gravity and microgravity sample on the left and right, respectively. 36

Figure 4-9 – Polished Series 1 samples that were not flushed with alcohol showing similar microstructures with terrestrial gravity and microgravity on the left and right, respectively. 37

Figure 4-10 – The terrestrial sample on the left shows the general microstructure at the 2 hour and 28 minute mark. On the right, is the microgravity sample showing four areas of where gypsum used to be. 39

Figure 4-11 – The top left and right images show a comparison of the terrestrial and microgravity microstructures, respectively, at 2 hours and 28 minutes of hydration. The bottom show a higher magnification of the microstructure for the terrestrial (left) and microgravity (right) sample. The hollow core is noted with the circle and arrow. 41

Figure 4-12 – EDS analysis of inside the gypsum exoskeleton at 2 hours and 28 minutes of hydration. 42

Figure 4 -13 – Just below the center of the image, a gypsum exoskeleton is seen with hydration products formed within the inside of the microgravity sample. At the top center of the image, there appears to be a similar formation that is more of cross-sectional view with the outside ring apparent, a slight gap, and then hydration products on the inside. 44

Figure 4-14 – A comparison of the polished surface microstructure at 6 hours and 6 minutes with the terrestrial sample on the left and the microgravity sample on the right. 45

Figure 4-15 – An EDS analysis looking at the differences in the hydration products within and composing the exoskeleton of the gypsum. 46

Figure 4-16 – A polished cross-section of the terrestrial and microgravity microstructure at 23 hours and 21 minutes, left and right, respectively.....47

Figure 4-17 – EDS analysis of the microgravity microstructure. a) The top graph shows the hydration products within the exoskeleton ring and b) the bottom graph shows the ring itself. 48

Figure 4-18 – A terrestrial sample seen on the left and the microgravity sample on the right revealing microstructures that have become more similar than seen previously.....49

Figure A-1 – On the top left is the clinostat machine. Four of the 50-mL vials can be supported at one time. On the top right is a prepared sample with the powder on the crystal bond on the needle tip. The bottom image is an SEM image looking down on the needle before the test.....55

Figure A-2 – On the left and right are pieces of gypsum that were in the static state and spun at 3 rpm in the clinostat, respectively. 56

Figure A-3 –. The image on the left is from the static condition for 5 minutes. On the right is a formation of a cluster of ettringite from hydration within the clinostat for 5 minutes.....56

Figure A-4 – C_3A and gypsum on the left and right, respectively, before alcohol exposure. 58

LIST OF TABLES

Table 3-1 – Sample mixture description and flush times.....21

Table 3-2 – Calculated average atomic numbers and backscattering coefficients for the main phases present in the study. All phases, excluding C_3A, are for their ideal bound water form. 23

Table 4-1 – Summary of the porosity measurements from analyzing twenty images per sample. 38

Table A-1 – Sample design and time spun on the clinostat 54

ACKNOWLEDGEMENTS

I would like to thank my advisor, Dr. Aleksandra Radlińska, for such an incredible opportunity to work on an amazing project and for her guidance throughout the start of graduate school. Moreover, I would like to thank my committee members Dr. Farshad Rajabipour, Dr. Sven Bilén, Dr. Barry Scheetz, and Dr. Richard Grugel for their insights and support as I further my academic experience. Also, this project would not be successful without the wonderful people at NASA and astronauts of Expedition 56. Thank you to Dr. Grugel at NASA's Marshall Space Flight Center for the countless important insights through his experience in material science and International Space Station research. Furthermore, I would like to thank my colleagues at Penn State for their advice and support. Specifically, I would like to acknowledge Juliana Neves for bringing me up to speed on the MICS project and getting me pointed in the right direction.

My experiences thus far at Penn State would have never been possible if it was not for my wonderful undergraduate research advisors at Utah State University. Dr. Andrew Sorensen and Dr. Marc Maguire provided multiple unique cementitious materials projects for me to be involved with. Moreover, I wouldn't be at Penn State if it was not for Dr. Robert Thomas for all the help in my undergraduate research, graduate school advice, and putting me in contact with Dr. Radlińska at Penn State.

Furthermore, I would like to thank my friends and family over the years for their continual support and pushing me to do my best. My parents, Adrian and Danielle, continually motivate me to set my goals high but enjoy the life I am living. Lastly, I would like to thank my grandfather, Peter, for being someone I will never forget and always look up to. I am truly surrounded by a wonderful support system in all directions. I would not be where I am today if it was not for the guidance received from all these individuals.

The Microgravity Investigation of Cement Solidification (MICS) project that this thesis is a part of is based upon work supported by NASA under award No. NNX17AC48G. Any opinions, findings, and conclusions or recommendations expressed in this material are those of the author(s) and do not necessarily reflect the views of the National Aeronautics and Space Administration.

Chapter 1

Project Background and Objectives

1.1 Project Introduction

On July 20, 1969 Neil Armstrong leaped from the Eagle lander and stepped foot on the Moon with the famous saying of, “that’s one small step for (a) man, one giant leap for mankind” (Loff, 2019). Since this historic event occurred 50 years ago as part of the Apollo program, there have been five other manned Moon landings with the last one occurring on December 11, 1972 (Loff, 2019). As time has gone on, the desire to go back to the Moon and beyond has grown. With the start of the Artemis program (the twin sister of Apollo and goddess of the Moon in Greek mythology), humans will be back on the Moon by 2024. Moreover, the goal is to have a sustainable human presence on the Moon in 2028 with the thought of going on to Mars in the 2030s (Dunbar, 2019).

Since the plan is to have these human space exploration missions for extended periods of time by the end of the next decade, there are some challenges that must be met. One of the most notable is the thought of building and maintaining resilient infrastructure for the humans to live in and be able to store equipment from the harsh environments present on these extraterrestrial bodies. The Moon for example, has an extremely poor atmosphere called an exosphere (leading the environment to act similar to a vacuum), temperatures ranging from -280°F to 260°F (-173ºC to 127ºC), and solar radiation effects (Planetary Science Communications Team, 2019a). Furthermore, the maximum temperature on Mars is 70°F (21ºC) and the minimum is -225°F (-142ºC). Mars also has strong wind storms that are known to suspend the dust in the atmosphere for months at a time (Planetary Science Communications Team, 2019b). All of these conditions

must be accounted for when planning for a sustainable presence on the Moon or Mars and are unlike anything that is experienced on Earth. This leads to a need for some fundamental research on the feasibility of using construction materials, such as concrete, to build pieces of infrastructure on extraterrestrial bodies.

The Pennsylvania State University is working in collaboration with NASA, CASIS, NIST, and industrial partners BASF, IPA, and Sauereisen to conduct the Microgravity Investigation of Cement Solidification Project (MICS). As part of the project, 8 kits, totaling 120 samples with a variety of constituents, were sent to the International Space Station (ISS) on the Orbital ATK OA-9E commercial resupply mission on May 21, 2018. The cement paste samples were mixed by astronauts on the ISS while simultaneously, identical terrestrial samples were mixed. The samples returned on the SpaceX CRS-15 on August 3, 2018 and were transported to NASA's Marshall Space Flight Center and the Pennsylvania State University for analysis.

The goal of the MICS project is to understand the influence of gravity on the solidification process of cement. This will help in furthering the ability of using a cement-like binder from in-situ materials to construct infrastructure on extraterrestrial bodies. The project is in direct alignment with the materials section (12.1) of the technology roadmaps that NASA has released (Vickers et al., 2015). Moreover, the solidification process is complex and not fully understood on Earth. The unique environment of microgravity can provide a novel approach to understanding the hydration of cement to further improve the sustainability of the material.

1.2 Research Objectives

The manufacturing of portland cements, such as ordinary portland cement (OPC), creates four main phases: tricalcium silicate ($3CaO{\cdot}SiO_2$: C_3S), dicalcium silicate ($2CaO{\cdot}SiO_2$: C_2S), tricalcium aluminate ($3CaO{\cdot}Al_2O_3$: C_3A), and tetracalcium aluminoferrite ($4CaO{\cdot}Al_2O_3{\cdot}Fe_2O_3$:

C_4AF). The amount of each phase can vary depending on the type of cement but typically range from 45 to 60, 15 to 30, 6 to 12, and 6 to 8 percent, respectively (Mehta & Monteiro, 2006). After the production of cement, calcium sulfate dihydrate, also known as gypsum ($CaSO_4 \cdot 2H_2O$: $C\bar{S}H_2$), is either added with the grinding of the clinker or afterwards at a replacement amount of about five percent. Gypsum plays an extremely important role in the early age kinetics, such as workability and set time, of portland cements.

C_3A is the most reactive of the four phases within OPC and its reaction upon the addition of water is instantaneous. This reaction of water with the C_3A is highly exothermic and can lead to an undesirable event called flash set where the concrete will harden extremely fast due to the rapid formation of various calcium aluminate hydrates (Mehta & Monteiro, 2006). In order to curve this rapid reaction, gypsum is added to OPC. When water is added to portland cement containing gypsum, there is still a rapid reaction of the C_3A with water, however, it becomes hindered rapidly by the gypsum through a mechanism that is still not fully understood (Joseph, Skibsted, & Cizer, 2019; Minard, Garrault, Regnaud, & Nonat, 2007; Myers et al., 2016) . This allows for the process of being able to mix the concrete, load it into the concrete truck, transport the mix to the job site, pour, and finish it all before it starts to set.

This research seeks to understand how the hydration of C_3A and gypsum pastes are influenced by gravity and lack thereof. It is apparent that the dissolution of gypsum and its interaction with the C_3A is an important reaction within portland cements and it is thought that the kinetics of these reactions will be influenced by a change in gravity level. Microgravity has been shown to minimize fluid convection and as cement reactions are highly exothermic processes, the mobility of the ions in solution will not be heavily influenced by convection patterns (McPherson et al., 1999). This leads to a hydration process that is predominantly diffusion driven in microgravity. To that extent, it is feasible to believe that there will be considerable differences between the hydration of the samples on Earth versus the ISS. This will

provide a novel approach to looking at the hydration process and trying to further understand the reaction on Earth.

It is noted that the goal for the infrastructure needed within the planned human space exploration missions is to make use of as much in-situ materials as possible. The cost of shipping material out of Earth's orbit in 2002 was estimated to be $10,000 per pound and to that point it is not feasible to bring everything needed from Earth to the Moon (Futron Corporation, 2002). SpaceX has significantly been able to lower the costs to around $1200 per pound or even lower depending on the type of rocket being launched ("Capabilities & Services," 2019). This is a significant reduction in shipping costs, but it is still not reasonable to think about shipping all the needed supplies from Earth. However, it is a feasible idea that any cement-like binder created with in-situ materials will go through a hydration process of some kind. Therefore, it is important to extensively study as many of the fundamental cement reactions that are known in microgravity with the anticipation of applying this knowledge to future cement-like binders. Two different proportions of C_3A and gypsum are studied within this work to help give a complete picture of what may be expected for similar reactions and further understand the more complex systems.

1.3 Thesis Outline

This thesis is broken up into four remaining chapters with the next, **Chapter 2**, being a literature review and background information on the tricalcium aluminate and gypsum reaction. **Chapter 3** will cover the materials used within the study and the mix designs. The third chapter will also discuss the characterization methods used. **Chapter 4** covers the results and discussion of the two different series of samples that were analyzed. Lastly, **Chapter 5** is a summary of the findings as well as the future work that is to come within the project. The **Appendix** of the thesis contains information on two minor supplemental studies that were done in support of the project.

To summarize the supplemental studies, a clinostat was used to try and mimic the results being seen in the microgravity sample and the anhydrous materials were subjected to prolonged alcohol exposure to see if there were any morphological differences.

Chapter 2

Literature Review

2.1 Reactions Associated with C_3A and Gypsum

The hydration products that form upon mixing C_3A and gypsum with water are dependent upon multiple variables. One of the most important variables affecting phase formation is the initial sulfate content (amount of gypsum). Others include the initial type of water used upon mixing, whether the sample is exposed to the CO_2 within the atmosphere, and temperature and humidity at mixing and curing. With control over these variables and the help of previous studies, the basic phases can be predicted fairly well. However, as in any cement-based system the kinetics are highly complex. In literature a certain sequence of reactions is often stated for simplicity and all the hydration products are a part of one of the two families.

In the hydration of C_3A and gypsum systems, two families form known as either the Al_2O_3-Fe_2O_3-mono (AFm) or the Al_2O_3-Fe_2O_3-tri (AFt). As seen in Figure 2-1, the AFm phases are built upon a $[Ca_2(Al,Fe)(OH)_6]^+$ main layers and an interlayer of $[X \cdot nH_2O]^-$ where X is a monovalent anion (i.e. OH^- or Cl^-) or half a divalent anion (i.e. SO_4^{2-} or CO_3^{2-}) and n can range depending on the phase (Baquerizo, Matschei, Scrivener, Saeidpour, & Wadsö, 2015; Joseph et al., 2019). AFt is similar to AFm, but there are more calcium ions and three X terms, typically SO_4^{2-}, which creates ettringite ($C_6A\overline{S}_3H_{32}$). Which of the phases that will form in a hydrating system depends on the saturation level of the various ions in the solution. The hydration of these systems is typically broken into three steps.

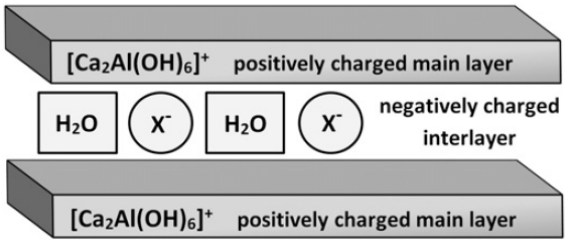

Figure 2-1 – A schematic showing the basic AFm structure (Baquerizo, Matschei, & Scrivener, 2016).

The first part of the reaction involves the initial mixing of water to a C_3A and gypsum system where there is a rapid reaction. It is given that there is an abundance of gypsum initially available so the hydration product that forms is ettringite as seen in equation (2-1) (Quennoz & Scrivener, 2012).

$$C_3A + 3C\bar{S}H_2 + 26H \rightarrow C_6A\bar{S}_3H_{32} \quad (2\text{-}1)$$

After the sulfate supply from the gypsum has been completely exhausted and there is still remaining C_3A in the system, it is favorable for the ettringite to react with the C_3A and form monosulfoaluminate (monosulfate or m-AFm) as seen in equation (2-2). The amount of bound water can change depending on relative humidity that the samples are exposed to and can range from nine to fourteen molecules (Baquerizo et al., 2015). This change in bound water leads to a slight change in the crystalline structure that can be seen through shifts in peak locations within X-ray diffraction. This reaction is also assuming the samples are protected from CO_2 because if they are not, the monocarboaluminate and hemicarboaluminate phases can form with a variety of bound water as well (Baquerizo et al., 2015).

$$2C_3A + C_6A\bar{S}_3H_{32} + 4H \rightarrow 3C_4A\bar{S}H_{12} \quad (2\text{-}2)$$

Once all the ettringite has reacted to form the m-AFm and there is still C_3A in the system, the hydroxy-AFm phases can form. If there is no C_3A in the system after the formation of m-AFm, then the hydroxy-AFm should not form (Pommersheim & Chang, 1988). At first, a variety

of different aluminate hydrates can form, again with varying bound water depending on the humidity, but the products are reported to turn into the more favorable state of hydrogarnet given enough time (C_3AH_6) (Black et al., 2006; Joseph et al., 2019).

$$2C_3A+21H \rightarrow C_4AH_{13} + C_2AH_8 \quad (2\text{-}3)$$

$$C_4AH_{13}+ C_2AH_8 \rightarrow 2C_3AH_6 + 9H \quad (2\text{-}4)$$

However, as will be shown later within literature and this work, all of these phases can be present in some manner; the reaction sequence is not perfectly chronological as is often stated and there are a lot of variables and conditions that influence these reactions. Moreover, the hydroxy-AFm phases (equation 2-3) are supposed to form first and then be converted into hydrogarnet at a later age. This process can be expedited and hydrogarnet can be visible towards the beginning of the reaction. In pure C_3A systems where a lot of heat is produced, and can be further increased with a low water to cement ratio, the formation of hydrogarnet initially is favorable (Pommersheim & Chang, 1986). This is an important point as a lot of heat can also be produced in a C_3A and gypsum system and the less gypsum in a system, the more reactive the C_3A will be and produce more heat. Furthermore, when this process is done in a microgravity environment where convection patterns are minimized limiting the ways to disperse the heat, a reaction favoring the formation of hydrogarnet is feasible.

2.2 Gypsum Dissolution and Phenomena within C_3A

Gypsum's role within cement is well known to prevent a flash set by hindering a rapid reaction of C_3A with water which would lead to the precipitation of calcium aluminate hydrates (hydroxy-AFm). The process through which gypsum dissolves is not something often looked at by researchers in the cementitious materials realm. However, the phenomenon of gypsum hindering the dissolution of C_3A has been a focus of research over the years within concrete

materials as it is an important concept within OPC. Historically, within OPC, gypsum has been added at relatively constant amounts of about 5% by weight but as society pushes towards more ecofriendly solutions, blended cements are becoming more popular. It is important that these are properly sulfated per the design of the blended cement and not just the ordinary portland cement component of the mixture. Not doing so can lead to undersulfation and may hurt the strength of the concrete among other issues (Scrivener, Juilland, & Monteiro, 2015). As such, a complete understanding of gypsums dissolution in a cementitious system is becoming more apparent as the mixtures continue to advance. Here, the process which gypsum dissolves will be discussed from perspectives outside cementitious research, as well as the phenomenon for gypsum hindering the rapid reaction of C_3A.

The dissolution of gypsum has been well studied as it is a fundamental mineral within the world. Outside the cementitious materials context, it has been noted to play a foundational role in drinking water, gypsum plaster, soil quality and plant growth, as well as the formation of karst (Zareeipolgardani, Piednoir, & Colombani, 2017). This has led to a lot of research looking at the dissolution process with a focus on the (0 1 0) cleavage plane, as this is the plane which exemplifies perfect cleavage (Bosbach & Rammensee, 1994; Fan & Teng, 2007; Pachon-Rodriguez & Colombani, 2013; Zareeipolgardani et al., 2017). The dissolution of gypsum can be described with the equation (2-5):

$$CaSO_4 \cdot 2H_2O \rightarrow Ca^{2+} + SO_4^{2-} + 2H_2O \qquad (2\text{-}5)$$

The method of studying this dissolution process varies between the scale of the experiment. Generally, flow cells are used for large scale experiments and smaller experiments at the microscopic level are done using atomic force microscopy (AFM). Zareeipolgardani et al. noted that historically the measured dissolution rates for the two methods do not coincide (Zareeipolgardani et al., 2017). However, this was noted as an expiremental issue that has to be

accounted for in the test method and instrumental set up. In doing so, the results from the microscopic and macroscopic level coincide well.

The dissolution of gypsum follows similar models for other minerals. Minerals typically form etch pits, and in the case of gypsum this occurs in a rhombohedral fashion on the (0 1 0) and (0 $\bar{1}$ 0) faces as seen in Figure 2-2 (represented by the ball and stick figure) and Figure 2-3 (AFM image). These etch pits were once thought to create a more reactive surface area, but are now viewed to be the start of a layer by layer dissolution process. (Lasaga & Luttge, 2001). In gypsum, once these etch pits form there is step retreat in both the [1 0 0] and [0 0 1] direction. Fan and Teng note the step retreat is faster in the [1 0 0] than in [0 0 1] no matter the degree of saturation within the system (Fan & Teng, 2007). It has been shown that the rate of dissolution of gypsum is a function of the degree of saturation. The more saturated the solution is, the slower the dissolution process and the life span of an etch pit increases (Zareeipolgardani et al., 2017).

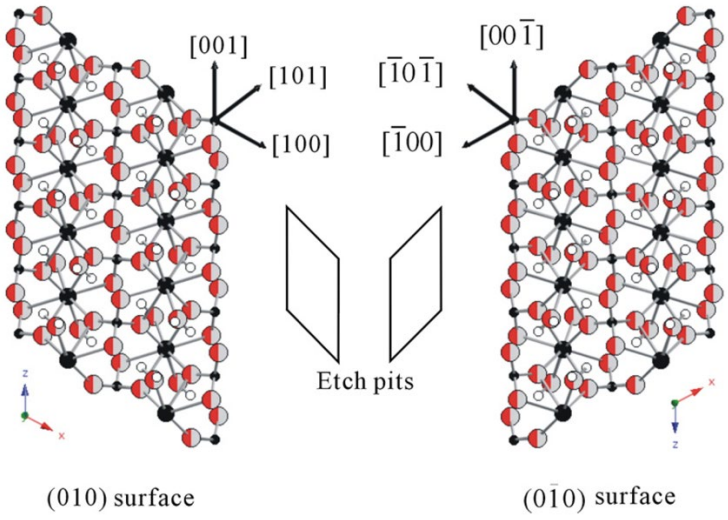

Figure 2-2 – An image from Fan and Teng showing the molecular structure of gypsum and how the etch pits form on the two surfaces (Fan & Teng, 2007). The calcium, sulfur, oxygen, and hydrogen are represented by the large black circles, small black circles, half colored circles, and small white circles, respectively.

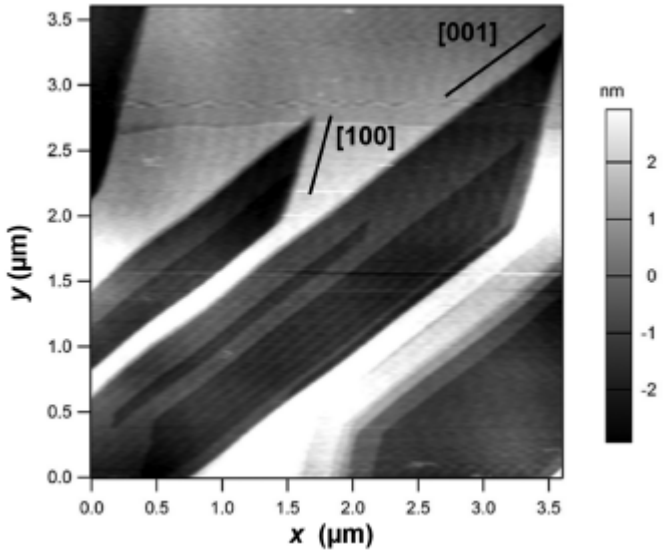

Figure 2-3 – An AFM image showing the etch pits that form with respect to the [1 0 0] and [0 0 1] direction (Zareeipolgardani et al., 2017).

The contribution of dissolution, diffusion, and convection are on the same order of magnitude for timescales in soft minerals, such as gypsum, which makes separating the effects of each challenging (Pachon-Rodriguez & Colombani, 2013). This is an important idea to note as this will be true for the Earth based samples within the MICS project. The story will be quite different for the samples in the microgravity environment as a diffusion-controlled process is expected due to minimized fluid convection and a lack of buoyancy. A study done by Pachon-Rodriguez et. al. tried to distinguish between these and obtain a pure dissolution rate of gypsum.

To get rid of the effects of diffusion and convection, the study by Pachon-Rodriguez et. al. developed a method to make use of holographic interferometry (Pachon-Rodriguez & Colombani, 2013). The study focused on the main cleave face of gypsum (0 1 0) in pure water as well as a combination of various salt solutions. The salt solutions were used to check if the ions would adsorb to the surface of the gypsum and inhibit its dissolution in some form. None of the salts used within the study would be of what is typically found in cement systems however they did show that dissolution of the gypsum can be significantly reduced with adsorption of ions

within the system. Hinderance of the dissolution of gypsum would be a highly undesirable event in a cementitious system as its role in preventing a flash set within concrete is crucial to the wide variety of mixtures used today.

A paper by Joseph et. al. summarizes the current state of knowledge on the history of the dissolution of C_3A being hindered with some connection to gypsum (Joseph et al., 2019). The authors provide a new theory for the phenomenon that differs from the other current proposed ones, as they propose that ettringite may not completely block the surface of the C_3A grains but provides enough coverage to slow the rapid reaction of C_3A. Here the current state of knowledge and previous studies will be expanded upon. This will cover the experimental methods that led to the development of the main theories and more detailed description of each of the research projects findings.

The phenomenon in gypsum in slowing the rapid reaction of the C_3A can be broken into two different categories of theories. The first one would be that there is a growth of some phase on the surface of the C_3A, which could be ettringite or hydroxy-AFm. The second category would be the adsorption of ions on the surface of the C_3A's active sites. Both categories of theories are nothing new and have been around since the mid 1900's. There is experimental evidence supporting and contradicting both, and up until recently it was starting to be agreed upon that the phenomenon was due to the adsorption of calcium and sulfate ions. However, recent work proposes and does not rule out an interaction with ettringite (Joseph et al., 2019).

A significant amount of research has been done on the setting of concrete in the mid 1900's as it an incredibly important aspect of concrete mixtures. Part of the findings throughout the years produced the ettringite barrier layer theory. This theory states that ettringite precipitates forming a thin film or gel-like layer around the C_3A inhibiting its dissolution (Seligmann & Greening, 1964; Stein, 1962). These findings were typically derived from the hydration products visible in x-ray diffraction and in combination of isothermal calorimetry. The use of a scanning

electron microscope (SEM) in cement research was still in early stages. Stein found in 1962 that this ettringite layer controlled the reaction by waters ability to transport either by diffusion or Poiseuille flow acknowledging that the layer formed is not necessarily completely closed tight (Stein, 1962). This is an important point that is historically forgotten as it is often stated that the ettringite barrier layer led to a diffusion-controlled ion transportation and doesn't acknowledge the Poiseuille flow statement.

In 1965, Stein expanded upon the previous study and looked at the hydration of C_3A and gypsum in suspensions and pastes. This study used techniques such as isothermal calorimetry, conductivity measurements and chemical analysis of solutions, X-ray diffraction (XRD), and SEM. The suspension and pastes proved slightly different theories of the hinderance effect, but both have common ground. It was proposed in both cases that there is a formation of an amorphous hydroxy-AFm layer that coats the surface of the grains. In suspension, that layer exists until most of the sulphate ions have been converted into ettringite. In pastes, the ettringite and hydroxy-AFm layer coexist on the grains until the ettringite recrystallizes into m-AFm. These findings were attributed to ettringite being the only found hydration product in early ages by XRD and that the corresponding heat evolution curve was too complex for just a single phase to be present.

A year later, it was refuted that ettringite could not cause this barrier layer and the slowing of C_3A was due to the adsorption of sulfate ions on the surface (Feldman & Ramachandran, 1966). However, there was little evidence backing this theory and it was not until 1977 that a paper noted this lack of evidence and investigated the theory. A short paper by Skalny and Tardos investigated the adsorption theory by means of looking at dissolution kinetics and electrokinetic behavior (Skalny & Tardos, 1977). They found that they also opposed the ettringite barrier layer theory on the premise that ettringite is formed by a though-solution mechanism and not by topochemical reaction as stated prior by Mehta (Mehta, 1976).

Not long went by before another study was released in 1979 that refuted the adsorption of sulfate ions and went back to the ettringite barrier layer theory (Collepardi, Baldini, Pauri, & Corradi, 1979). Within the study they used isothermal calorimetry and thermogravimetric analysis (TGA) to look into the hinderance of C_3A dissolution by sulfate adsorption using different types of sulfates, namely gypsum and sodium sulfate. Their results showed that only the gypsum hindered the dissolution and that the sodium sulfate had no effect on slowing the dissolution process. On that premise, they concluded that sulfate adsorption could not be the reason for such phenomenon and that the formation of ettringite from gypsum is the reason. They note that ettringite may be formed from a through-solution mechanism, but that it forms preferentially on the surface of the C_3A grains.

Minard supported a modified version of the adsorption theories noting that the hinderance is likely due the adsorption of calcium and/or sulfate ions (Minard et al., 2007). The experiment made use of an isothermal microcalorimeter that was able to mix the sample within the calorimeter to register the early-age reactions and coupled the measurement with electrical conductivity. These techniques in combination with XRD and SEM micrographs showed that ettringite does not have a strong enough presence on the surface of the C_3A grains to limit the reaction rate. It is noted that there is an initial formation of an AFm phase on the C_3A surface, however, this phase is also present in pure C_3A systems where there is no hinderance of the dissolution rate. Therefore, they concluded that the adsorption of the calcium and/or sulfate ions was the most plausible explanation.

Work by Myers et. al. took a different approach into investigating the adsorption phenomena in C_3A dissolution (Myers et al., 2016). In the experiment they were able to determine zeta potentials and pH of a variety of C_3A mixtures. It is shown that the isoelectric point of C_3A occurs at a pH of 12. Moreover, there is no change in surface charge suggesting that adsorption is not S or Ca alone and that it is in fact a Ca-S ion pair complex that is causing the

retardation of dissolution. They also showed that the precipitation of phases on the surface of the C_3A are not responsible for any substantial change in the zeta potentials meaning that it is dominated by the Ca-S ion pair complexes.

An intensive study by Geng et. al. using a variety of techniques found that the ettringite formed on the surface of the C_3A is highly porous and would not provide a diffusion barrier preventing the dissolution (Geng et al., 2018). A comprehensive list of the methods are SEM, scanning transmission x-ray microscopy (STXM) and aluminum K-edge x-ray absorption near edge structure (XANES), x-ray ptychography, wide-angle x-ray scattering (WAXS) and small-angle x-ray scattering (SAXS), and transmission x-ray microscopy (TXM). The use of such techniques allows for high resolution and quantitative data. One of the main takeaways from the study was the porosity of the ettringite on the surface of the C_3A. In confined spaces the porosity is found to be 53-67% and in a more open environment a porosity of 73-81% was found which suggested that the retardation effect comes from the adsorption of the calcium and sulfate complexes on the surface, as previously reported.

The most recent theory reported in literature by Joesph et. al. pushes back on the theory of calcium and/or sulphate adsorption and goes back to the formation of ettringite on the surface being a reason for the hinderance (Joseph et al., 2019). Quantitative data was collected through the use of isothermal calorimetry, TGA, and solid-state NMR. Using this data and a cement microstructural modeling platform, CemRS, they were able to predict well the heat evolution curve, degree of hydration, and dissolution rate of a wide variety of C_3A and gypsum systems. Their model also accounted for changes in fineness of the C_3A. The authors note that their model and equations used could also be explained by an ettringite layer forming on the C_3A surface. This is stated to be different then the ettringite barrier layer theory as that theory was mainly composed of creating a barrier which ions must diffuse through. The theory reported here by Joseph et. al. said the ettringite layer formed merely hinders the dissolution rate.

Overall, these theories have continued to develop over the years with arguments and experimental data on both the adsorption and precipitation sides. While there is still a need for definitive evidence, it had been mostly agreed upon that the dissolution hinderance within C_3A and gypsum systems has something to do with adsorption. The recent paper by Joseph et. al. addresses how ettringite may provide a slowing effect but does not note the experimental data showing just how porous the surface coverage of ettringite is as reported in the Geng et. al. study (Geng et al., 2018; Joseph et al., 2019). Within computational modeling there are inherent assumptions that must be made which does not always correctly account for what is shown in experimental data. The hydration of these C_3A and gypsum systems are complex as anything within cementitious materials with questions that still need to be answered. The reported literature is essential in helping deduce some of the phenomena seen within the C_3A and gypsum samples within the MICS experiment.

2.3 Published Cement Microgravity Solidification Projects

The history of cement solidification projects in a microgravity environment is quite small and at a very fundamental state right now. The MICS project is the first in-depth research experiment done on the ISS to look at cement hydration. Research off the ISS is limited to a few studies conducted upon a parabolic flight. In these studies, a plane is able to ascend at a steep angle of around 47 degrees where it shuts off the engines and levels out for approximately 20 seconds before restarting the engines and continuing on its flight (Lei et al., 2016). During the time when the engines are off, a freefall effect is created that mimics microgravity. The experiments conducted within the parabolic flight study look at instantaneous ettringite precipitation in portland cement mixtures as no other hydration products had formed within the first 20 seconds. The papers note the difference microgravity and the combination of

polycarboxylate superplasticizers (PCEs) have on the morphology of the ettringite (Lei et al., 2016; Meier & Plank, 2016; Meier, Sarigaphuti, Sainamthip, & Plank, 2015). No other hydration products have been reported in literature outside of the MICS project.

Within the MICS project, a recent paper reported the results of a tricalcium silicate (C_3S) paste that hydrated on the ISS and compared to an identical Earth-based sample (Moraes Neves et al., 2019). The authors note that due to lack of buoyancy, increased trapped air and minimized bleeding and sedimentation are present in the microgravity sample. The crystal morphology of the portlandite (CH) crystals also varied from microgravity and terrestrial gravity with the microgravity samples being larger and more plate like as seen in Figure 2-4. This is attributed to the reduced bleeding effects within the microgravity sample leading to a higher effective water-to-cement ratio and more space for the crystals to precipitate in. Research of the fundamental pure components within OPC is a necessary first step to understand the more complex mixtures that are a part of the MICS project with a goal of helping formulate a binder using in-situ planetary materials.

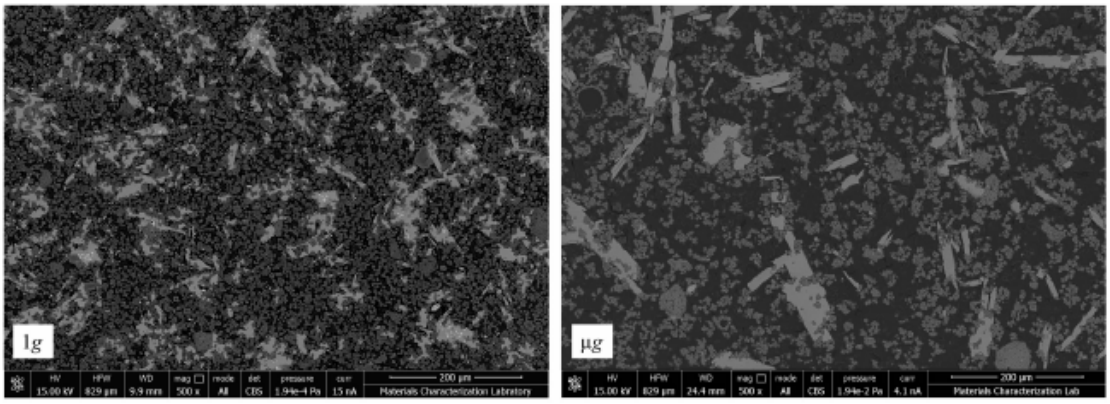

Figure 2-4 – An image from the published MICS C_3S paper showing the difference in porosity, C-S-H, and CH (Moraes Neves et al., 2019).

Chapter 3

Materials and Characterization Methods

3.1 Pouch Design and Mixing Procedure

NASA has a set of safety standards for conducting experiments onboard the ISS. This includes having multiple layers of containment for any ongoing experiment to mitigate the chances of a spill that would be hard to contain in the absence of gravity. The plastic pouches that were used for the MICS project counted as one level of containment (Figure 3-1 and Figure 3-2). The plastic pouches were stored within a sealable bag, expect for the time when the experiment was executed. The sealable bag was stored yet within another, larger sealable bag. The samples were mixed on the ISS within a portable glovebox, which also constituted a layer of containment during that process (Figure 3-1).

Figure 3-1 – Astronaut Alexander Gerst is mixing one of the MICS samples within the glovebox on the Maintenance Work Bench on the ISS (NASA, 2018).

The pouches implemented a technology called Burst Pouches®, where the seal in between the compartments can be burst open. This allowed for the samples materials to be kept separate until the desired mixing time. All of the samples were prepared in two-compartment or

three-compartment pouches depending on whether or not alcohol was needed to arrest the hydration of the cement paste (Figure 3-2). In either case, the desired materials were carefully measured and placed within the pouch and sealed by an external laboratory.

In order to start the mixing procedure, the outside edge of the water filled pouch is rolled up, like deflating an air pad, until enough pressure was reached within the pouch to burst the middle seal. With the help of a rubber spatula, all the water was emptied from the water compartment into the compartment containing the cement powder. The powder was mixed with the water through a combination of kneading with the hands and the spatula to create a homogenous mixture. After the water and cement had been thoroughly mixed, a plastic clip was added to the pouch to contain the material at the end of the compartment.

Figure 3-2 – On the left is an example of a three-compartment pouch that has been mixed, clipped, and flushed with alcohol. On the right is a two-compartment pouch that has been mixed and clipped. After the samples were mixed they were placed in the sealable bag also seen in the right image.

3.2 Materials and Sample Design

Cubic C_3A synthesized by Mineral Research Processing in Meyzieu, France and gypsum from Sigma-Aldrich were used in this study. The purity of the components was checked with XRD and a small amount of free lime (CaO) was apparent (~1%) in the C_3A. It should be noted that when viewing the phase diagram for calcium aluminates there will always be some free lime produced in the creation of C_3A (Taylor, 1990). The particle size distribution for the C_3A and gypsum can be seen in Figure 3-3. Isopropanol was used as the dispersant on a Mastersizer 3000. The Dv 50 for the C_3A and gypsum was 5.34 µm and 26.4 µm, respectively. The C_3A and gypsum were mixed with lime water that was produced with calcium hydroxide from Alfa-Aesar with a concentration of 15 mmol/liter. To arrest the hydration, 99% isopropanol was used and the amount of alcohol in the pouch was ultimately determined to be just over nine times the volume of the paste, due to safety limitations of conducting science experiments on the ISS.

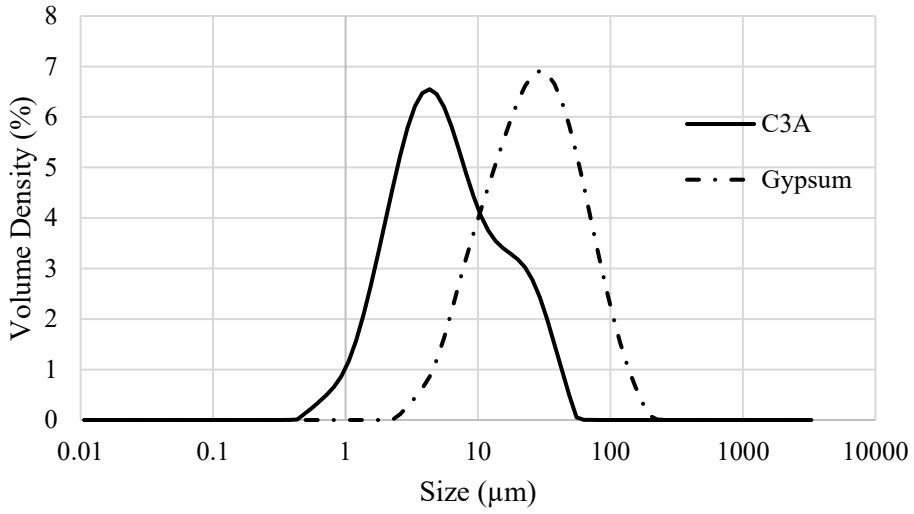

Figure 3-3 – The particle size distribution of the C_3A and gypsum used within the study.

The three-compartment pouches were used to arrest the hydration at various times during the first day to evaluate time-dependent microstructural development. All the pouches that were

designed to be flushed with the isopropyl alcohol were meant to be done at 3 hours, 7 hours, and 24 hours after mixing. However, as the astronauts were dealing with a lot of samples, the flush times ranged from about an hour before to an hour after the designed time. The terrestrial specimens were created and mixed to match the identical flush times as the ones the astronauts did. This allowed for a direct comparison of the microstructures at the same time in the hydration process. Table 3-1 shows the mixture description and the actual flush times for the two sets of samples within this study.

Table 3-1 – Sample mixture description and flush times.

Mixture ID	Mixture Description	Water to Cement	Flush Times				
Series 1	80% C_3A and 20% Gypsum	1.0	2.18 hours	2.58 hours	6.23 hours	22.97 hours	253 days
Series 2	90% C_3A and 10% Gypsum	1.0	2.47 hours		6.10 hours	23.35 hours	385 days

3.3 Scanning Electron Microscopy (SEM)

Both fractured and polished surfaces were viewed for the samples within the study to identify any morphological differences in the dissolution and formation of phases, as well as look at the distribution of the phases. Most of the images were acquired on a Hitachi S-3700N SEM but a few images were taken on a FEI Q250 ESEM. All the samples were viewed at an accelerating voltage of 15 kV, a working distance of 10 mm, and an image acquisition time of approximately 1.25 minutes. The samples viewed on the Hitachi SEM were viewed in low vacuum with a chamber pressure of 30 Pa. It should be mentioned here that in low vacuum, the Hitachi SEM was limited to viewing the sample with the backscattered electron (BSE) detector.

The samples that were epoxied and polished were not vacuum dried prior to epoxy impregnation in fear of altering the sensitive AFm phases. The samples were cut to size and left

in an argon purged glovebox for a week before epoxying to dry naturally as well as possible. As the samples were rather soft and weak, especially at the early ages, they were mounted in a soft grade (*L.R. White*) resin by adding a small amount to the cup and placing the sample in. This small amount of epoxy was enough for capillary forces to pull up the epoxy within the sample giving the entire sample a wet look before filling the cup the rest of the way with epoxy. After the sample was mounted in epoxy, the samples were ground through a series of silicon carbide papers starting at a 30 μm grit and proceeding down to a 0.25 μm diamond paste on a rotary lapping wheel with a slow speed of no more than 100 rotations per minute to avoid overly abrasive polishing.

3.3.1 Image Analysis

As can be seen in Figure 3-2, the samples were rather small with a length of roughly 75 mm, width of 25 mm, and a thickness of 3 mm. To that extent, acknowledging that the feasibility of redoing one of the microgravity ones is rather inexistent, the amount of sample used for a test was conserved. To help save on use of the amount of sample used in each experiment, the ones that were epoxied and polished down to look at the overall cross-sections were also used for porosity measurement through an image analysis technique capable of correctly calculating the area of porosity in a given image.

An 8-bit SEM image is a compilation of pixels with grey scale values ranging from 0-255. This is possible as the electrons interact with the sample as a function of the average atomic number. The higher the average atomic number, the higher the greyscale value. This concept is often displayed by the backscattering coefficient. For an individual element the backscattering coefficient can be calculated with equation (3-1) which is displayed as (Zhao & Darwin, 1992):

$$\eta = -0.0254 + 0.016 \cdot Z - 1.86 \cdot 10^{-4} \cdot Z^2 + 8.3 \cdot 10^{-7} \cdot Z^3 \quad (3\text{-}1)$$

Where η represents the backscattering coefficient and Z is the atomic number of a given element. The backscattering coefficient of the phase of interest (e.g. C_3A) is the summation of the weight fraction of each element (calcium, aluminum, and oxygen) in the phase multiplied by its respective backscattering coefficient. This coefficient represents the ratio of electrons that are backscattered and picked up by the detector over the number that are emitted and hit the target sample. When this was done for the C_3A and gypsum sample, the calculated backscattering coefficient for each phase was obtained and displayed in Table 3-2. The contrast between the phases is related to the relative difference in BSE signal and is calculated with equation (3-2) (Zhao & Darwin, 1992):

$$\text{Contrast} = \frac{\eta_1 - \eta_2}{\eta_1} \tag{3-2}$$

Where η_1 and η_2 represent the backscattering coefficients for the phases of interest. The lower the contrast value, the harder it becomes to distinguish the differences between the phases.

Table 3-2 – Calculated average atomic numbers and backscattering coefficients for the main phases present in the study. All phases, excluding C_3A, are for their ideal bound water form.

Phase	Average Atomic Number	Backscattering Coefficient	Relative Position Ordered from Most Bright to Least Bright
C_3A	14.339	0.1639	1
C_3AH_6	12.304	0.1402	2
$C_4A\bar{S}H_{12}$	11.664	0.1324	3
$C_6A\bar{S}_3H_{32}$	10.703	0.1208	4

Image-based calculation of porosity relies on thresholding the image by establishing a greyscale threshold, where everything below a certain greyscale value is to be regarded as porosity and everything above should be a hydration product or anhydrous material. The software then creates a binary image where anything viewed as porosity is turned to a black pixel and everything else is a white pixel. Once the image is converted to the binary image, the percent area of the black and white pixels can be calculated. There have been multiple methods developed

over the years to conduct this type of analysis to mitigate relying on personal judgement. Often what appears to be the true boundary of a pore, or phase, may not necessarily be accurate, as there is an interaction issue with the electrons that are being produced at these boundaries.

The more recent method developed to conduct the porosity image analysis is known as the overflow method and was introduced in 2006 (Wong, Head, & Buenfeld, 2006). In this method, the cumulative greyscale curve is plotted based on the regular greyscale histogram. Subsequently, two tangent lines can be drawn as seen in Figure 3-4. The value on the x-axis where the lines cross is regarded as the greyscale value to be used for thresholding. This method was already used within the MICS experiment on a tricalcium silicate (C_3S) paste which was also compared to the data received from Mercury Intrusion Porosimetry (MIP) and produced agreeable results (Moraes Neves et al., 2019).

The image acquisition process for this set of analysis involved acquiring a set of 20 images at a magnification of 500×. Each pixel within the image represented 0.12574 μm. Areas within the image that were smaller than 10 pixels were regarded as noise and not included in the calculated area. This equates to ignoring regions with a theoretical circular diameter of 0.45 μm and determines the smallest pores size considered within the analysis. To perform the analysis on the images, a script was written in MATLAB following the procedure and information provided (Wong et al., 2006). To ensure a sufficient number of images were taken to be statistically significant, equation (3-3) was used to solve the number of images needed to be 95% confident that the sample mean porosity is within 10% of the true mean porosity:

$$n = \frac{t_\alpha^2 * \sigma^2}{\delta^2 * \mu^2} \tag{3-3}$$

Where t_α is 2.093 based off a two-tail test with a degree of freedom of 19 and a 95% confidence level, σ is the sample standard deviation, δ is the margin of error (expressed as a decimal), and μ is the sample mean.

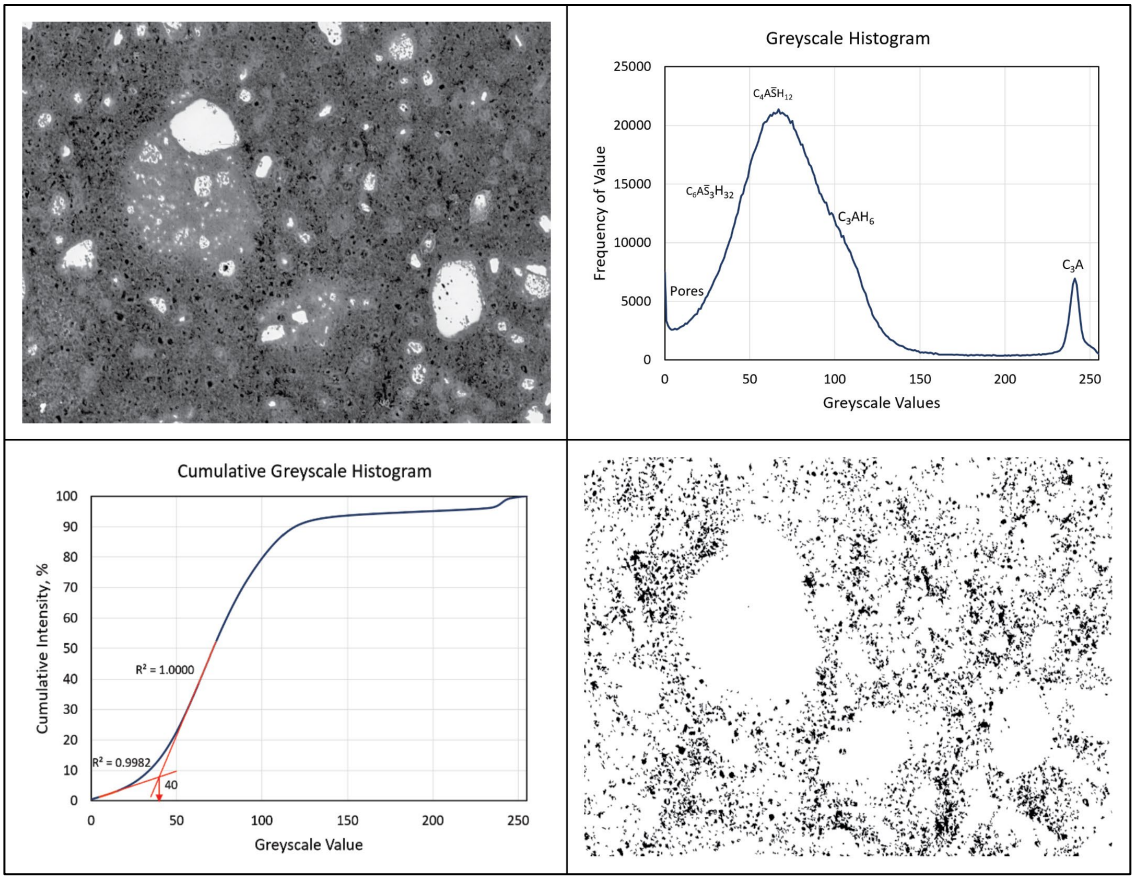

Figure 3-4 – The process for thresholding an image is shown starting at the original image. The typical greyscale histogram in the top right is converted into a cumulative curve in order to apply the overflow method. The original histogram shows a slight shoulder on the right side of the major hump, which would be the characteristic location of the C_3AH_6. The two linear lines are drawn until their intersection which leads to the greyscale value of 40 used to produce the final binary image for calculating the area of porosity.

3.4 X-Ray Diffraction (XRD)

The phases within a hydrated C_3A and gypsum system, particularly the ones within the AFm category, do not have well reported crystal structures resulting in the XRD data being rather qualitative. Samples were analyzed in a Bragg-Brentano θ-θ geometry setup with a PANalytical X'Pert Pro MPD. CuKα radiation was generated with 45 kV and 40 mA generator settings. Data was collected from a continuous scan from 5° to 70° 2θ on a spinning stage at one rotation per

second, a step size of 0.0130°, and time per step of 160 seconds. For optics, soller slits of 0.04 rad and a fixed divergence slit of 0.0625º were used with a nickel filter.

In an effort to reduce any possible effects of carbonation, the samples were stored within a nitrogen purged glovebox with a transfer chamber. The samples were crushed in the glovebox by hand using a mortar and pestle. The samples were then prepared with a front load, airtight dome sample holder within the glovebox (Figure 3-5). The holder was then transported from the glovebox to the XRD machine for analysis. The scan time was increased, and the step size was decreased in an effort to account for the loss of resolution due to the dome on the sample holder. The data obtained is rather qualitative and used to identify the phases present (in this case just in Series 1) as the crystalline structures for the AFm phases are not well defined (Joseph et al., 2019).

Figure 3-5 – A prepared XRD sample within the airtight dome sample holder.

Chapter 4

Results and Discussion

4.1 Series 1 Results and Discussion

The phases present in the terrestrial gravity and microgravity Series 1 samples were found with XRD to discern phases when viewing the microstructure through a SEM (Figure 4-1). The XRD patterns for the two gravity levels show that similar phases formed in both samples, however, there are differences in the peak intensities at the given times. Due to the poor reported crystalline structure of the AFm phases and the possibility of sample prep errors it is not possible to compare peak intensities or attempt a Rietveld refinement. However, some important points can be made in the identification of the phases.

The main m-AFm peak (9.8º 2θ) often has a slight shoulder on the right-hand side at early ages before a distinct peak starts to form in the sample that was never flushed with alcohol. It was initially assumed the m-AFm was dehydrated from the characterized m-AFm12 to the m-AFm10.5 due to relative humidity of the samples in the nitrogen purged glovebox (Baquerizo et al., 2015). The reported peak location for m-AFm10.5 within Baquerizo et. al. overlaps with the hemicarboaluminate peak and since extreme efforts were taken to prevent the samples from being exposed to CO_2, the hemicarboaluminate phase was not expected. However, after raising the humidity within the glovebox to well above the absorption point for m-AFm10.5 to uptake more water molecules to m-AFm12 and rescanning the sample, it was concluded that the slight shoulder was due to the hemicarboaluminate peak as the peak did not disappear as one would expect. This can be explained by the slight amount of air that is present in the pouches from the initial packaging as they were not packaged in a gas-purged glovebox. The amount of CO_2 in the

pouch is minimal, because if it was abundantly present it would drive a further conversion of the m-AFm to the hemicarboaluminate phases (Matschei, Lothenbach, & Glasser, 2007). This is an important finding within the project and needs to be kept in mind. In any future experiments, packaging should be performed in a CO_2 free environment.

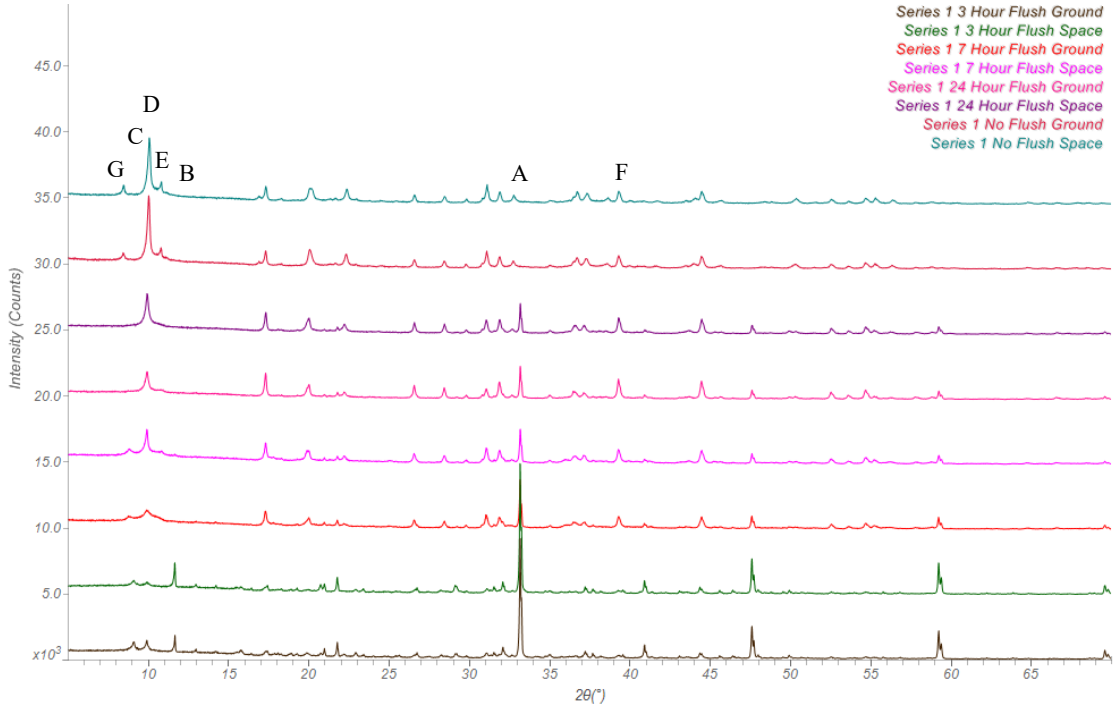

Figure 4-1 – The XRD patterns for the Series 1 samples alternating terrestrial gravity and microgravity with the age of hydration increasing from the bottom to top. The letters marking the main peaks represent (A) C_3A, (B) gypsum, (C) ettringite, (D) m-AFm, (E) hemicarboaluminate, (F) hydrogarnet, and (G) hydroxy-AFm (C_4AH_{19}).

4.1.1 Microstructural Differences at 2.18 and 2.58 Hours

Two set of samples with slightly different flush times were analyzed for both the terrestrial gravity and microgravity samples within Series 1. As a first step, the samples fractured surfaces were viewed with the SEM to identify any morphological variations between the two different gravity environments. Figure 4-2a and Figure 4-2b show a comparison of typical pieces of gypsum seen in the two samples that were flushed at the 2 hour and 11 minute mark and the

environment around the gypsum. The state of the gypsum in the terrestrial sample at this time is rather smooth with a few minor striations. This matches the reported literature that the dissolution of gypsum is a layer by layer process. Furthermore, the terrestrial sample typically has a surface that is free of hydration products, except for the occasional ettringite needles.

For the microgravity sample, the gypsum is considerably more striated throughout the sample and it becomes a site of ettringite growth. As can be seen on the top piece of gypsum in the microgravity sample (Figure 4-2b), it has a fuzzy look to it due to the growth of ettringite. It has been noted that the kinetics of the dissolution of the C_3A and gypsum is a function of the saturation level of fluid in the paste and also that calcium preferentially leaves the C_3A, resulting in a alumina rich layer on the surface (Myers et al., 2016). The mixtures within this study were supersaturated with respect to calcium due to the lime water and undersaturated with respect to sulfate and alumina, which would slow the dissolution of calcium ions from the gypsum and C_3A. In the terrestrial sample, the surface of the gypsum was continually cleaned of the ions due to convections patterns and buoyancy effects, where in the microgravity sample the movement is diffusion controlled. This may lead to a preferential dissolution of sulfate from the gypsum and demand as the ettringite grows on the surface leading to the striations that are seen.

The state of the gypsum in the microgravity sample is varied and the differences are seen throughout the matrix. Figure 4-2c and Figure 4-2d show other areas of what was likely the past location of piece of gypsum. Figure 4-2c shows a few remaining large slivers of gypsum with ettringite growth in the vicinity. Figure 4-2d shows a piece of striated gypsum in the bottom, but in the middle is an area that has the same long, plate-like morphology as gypsum that now looks like a cloud of hydration products.

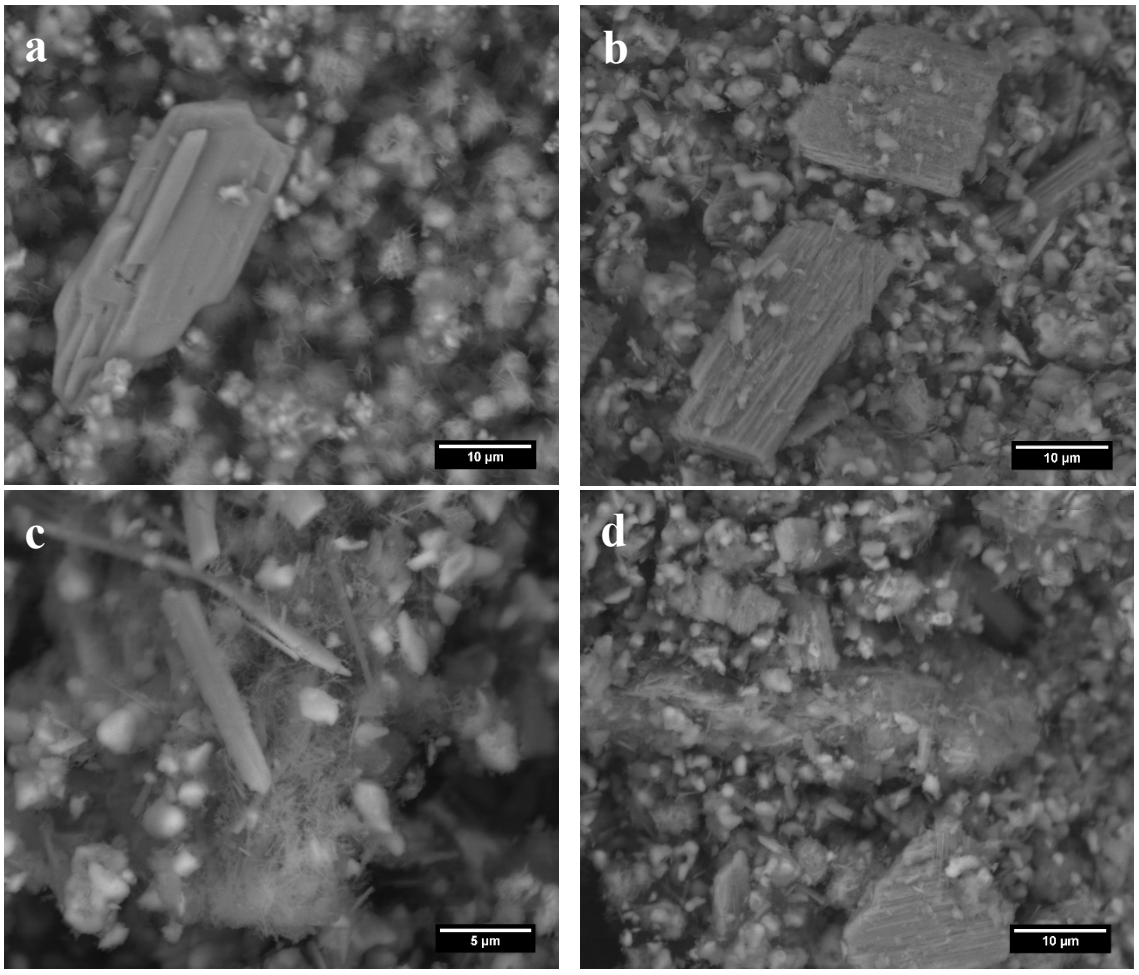

Figure 4-2 – a) Shows a piece of gypsum from the terrestrial sample after 2 hours and 11 minutes of hydration. It has a smooth surface with minimal striations. b) Shows two pieces of gypsum from the microgravity sample at the same 2 hour and 11 minute time. The gypsum in the microgravity sample is heavily striated and the top piece has growth of ettringite. c) Dense ettringite growth with very little gypsum remaining. d) A cloud of hydration products shows the past site of an original piece of gypsum.

In the microgravity sample, a few micrometers away from the gypsum, clusters of AFm hydration products are typically seen. The clusters are typically not seen away from the gypsum in microgravity, which leads to the formation of a sample that lacks a uniform distribution at these early ages. This is not to say that the AFm phases are not elsewhere within the matrix, as there is a rapid reaction upon the addition of water to the powder and then the astronauts promoted the movement of ions by mixing the sample, but the dominant cluster formation is near

the gypsum. As hydration in microgravity is diffusion controlled, the highest density of sulfate will be right around the gypsum (hence the ettringite growth on the surface) and a lower density of sulfate will be available slightly away from the gypsum. This difference in sulfate concentration will lead to the formation of the AFm phase and not ettringite. The opposite is seen for the terrestrial sample. The AFm plates are uniformly distributed throughout the microstructure. The initial high heat release would promote fluid convection allowing for a uniform fluid chemistry throughout the sample as it starts to solidify and form hydration products.

Fast forward 24 minutes in the hydration process to the 2 hour and 35 minute mark and looking at the gypsum in the terrestrial sample reveals that the gypsum is slightly more striated than it used to be (Figure 4-3). However, it is still not as striated as seen in the microgravity sample. Moreover, the microgravity sample is just as striated as before, but typically has a denser rim of ettringite growth on it. It can also be seen in Figure 4-3 that striations are not just seen at the surface of gypsum but exist all the way through when it is viewed looking down on the [0 0 1] direction. This image also shows the expected cluster of AFm right near the gypsum.

It was noted in the microgravity sample at 2 hours and 11 minutes of hydration that there were areas that looked like the past place of a piece of gypsum that have now been filled in with hydration products (Figure 4-2d). At 2 hours and 35 minutes of hydration, Figure 4-4 shows a large area of AFm plates (roughly 75-micron diameter). It is presumed that the area noted previously as a past piece of gypsum exhausted all the sulfate in vicinity, leading the ettringite to turn into AFm phases. As the sulfate is exchanged by the ettringite to form the AFm plates, it reacts with the remaining C_3A particles and spreads outwards. This process shows how minimized fluid convection and diffusion-controlled hydration process causes a nonuniform microstructure at these early ages in microgravity. The ions in the solution are suspended around the decomposing phases and have minimal movement compared to Earth based systems.

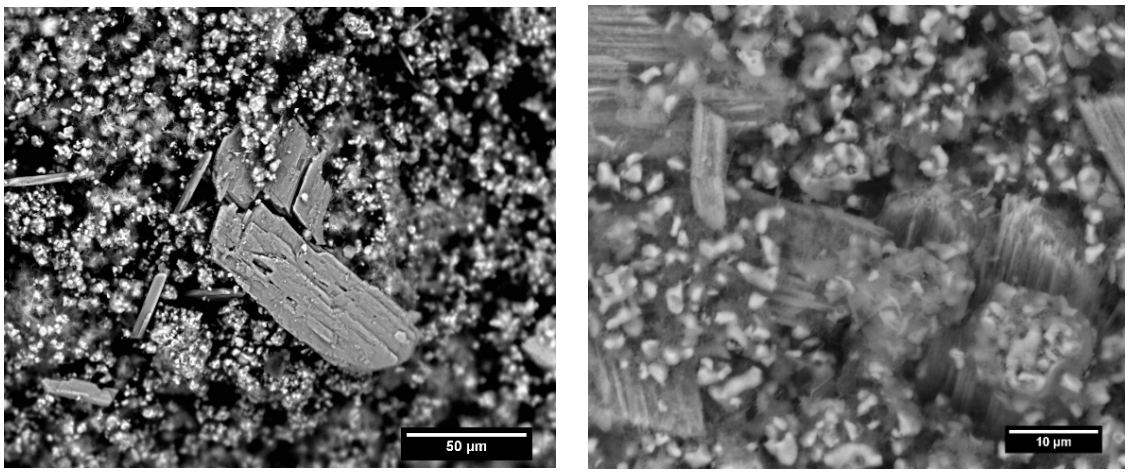

Figure 4-3 – On the left is a slightly striated gypsum crystal from 2 hours and 35 minutes of hydration on Earth. At the same hydration time, the gypsum in the microgravity sample is heavily striated with substantial ettringite growth on it and showing the AFm clusters nearby.

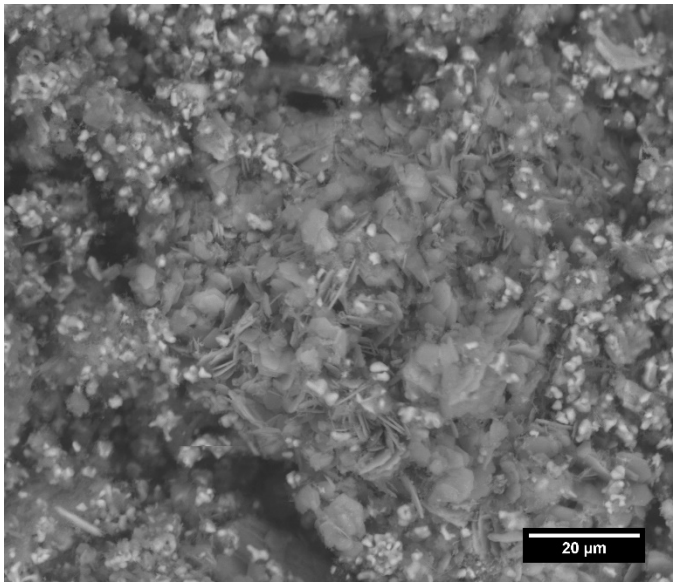

Figure 4-4 – A large area of AFm plates that likely used to be the place of a piece of gypsum.

The microgravity and terrestrial gravity samples that hydrated for 2 hours and 35 minutes had enough structural integrity that some of the pieces could be epoxied and polished. The observations from the fractured surfaces are further supplemented through the polished cross-sections. One of the first observations that stands out when comparing an image of both samples is the difference in the density. The terrestrial sample has a more developed microstructure

showing a higher degree of hydration with a few pieces of gypsum remaining (Figure 4-5). The state of the gypsum appears to have a rather clean surface with no substantial growth on it. The overall microstructure in the terrestrial sample is uniform, which matches the observations of a lack of the cluster formations in the fractured surfaces. The microgravity sample is quite different with areas that are concentrated.

Figure 4-5 also shows the microgravity sample on the right and the image reveals a microstructure with areas of significant fluctuation in development. The middle parallelogram shows a lack of gypsum and any sign of a past piece, while also having large grains of C_3A. The area is very porous and shows a lack of significant hydration product formations. The two triangles (top and bottom of the left side) show a microstructure containing gypsum that appears to have some rough edges, but gives the impression to be intact overall. Lastly, in the bottom right is an area that is more developed then the rest of the microstructure seen in the image. Upon closer inspection of the area, what looks like the cross-section of gypsum is now an area of dense hydration products. The C_3A around this point is also starting to develop a noticeable ring of hydration products covering the surface grains. The uniformity of the structure in the microgravity environment is highly dependent upon the particles in the area, since the overall reactivity is a function of the surface area of the grains.

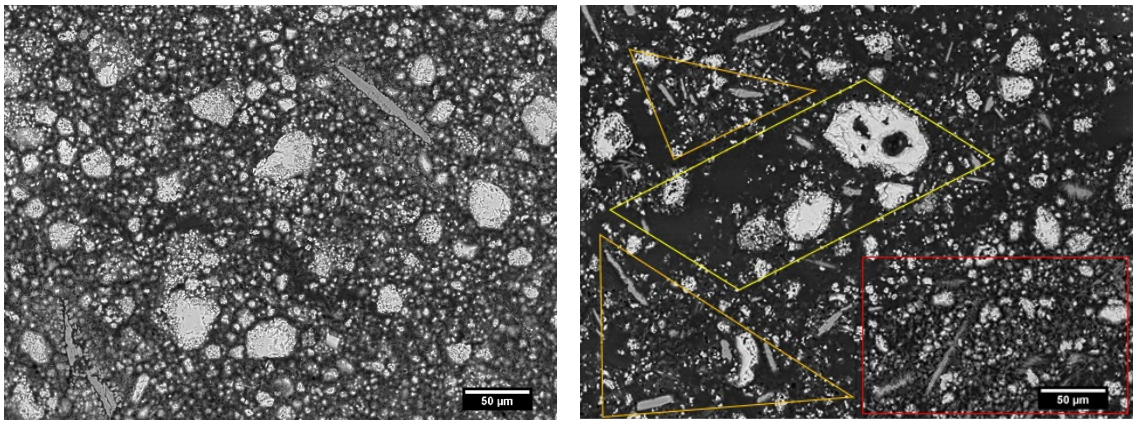

Figure 4-5 – On the left is the polished cross-section of the terrestrial sample that hydrated for 2 hours and 35 minutes and on the right is the microgravity sample at an identical time. The micogravity sample lacks a uniform distribution of hydration products.

4.1.2 Microstructural Differences at 6.23 Hours

The next set of samples analyzed were hydrating for 6 hours and 14 minutes for both the microgravity and terrestrial gravity environment. At this point in the hydration process, the gypsum has been exhausted in both systems and a denser and structurally sound microstructure has developed. From a lower magnification image it is apparent that lack of buoyancy in the microgravity samples causes air to be trapped within the matrix and air bubbles can be seen occurring frequently. This is a concern for future use of binders in extraterrestrial context, as entrapped air, or voids, will result in formation of weak points in the system. Air can be desirable in the sense of entrained air which has controlled bubble sizes of 0.05 to 1 mm with correct spacing as this helps with freeze-thaw durability (Mehta & Monteiro, 2006). It should also be noted here that the gravity of the Moon ($1.62 \frac{m}{s^2}$) and Mars ($3.711 \frac{m}{s^2}$) would still promote some buoyancy of the bubbles which may be enough to help get them out of the viscous paste mix. Analysis of whether the gravity levels of the Moon and Mars are enough to promote the air releasing for the viscous paste is yet to be examined. Figure 4-6 shows a comparison of the microstructures viewed from 30×. At this magnification the microstructures appear to be very similar with the microgravity one appearing slightly more porous.

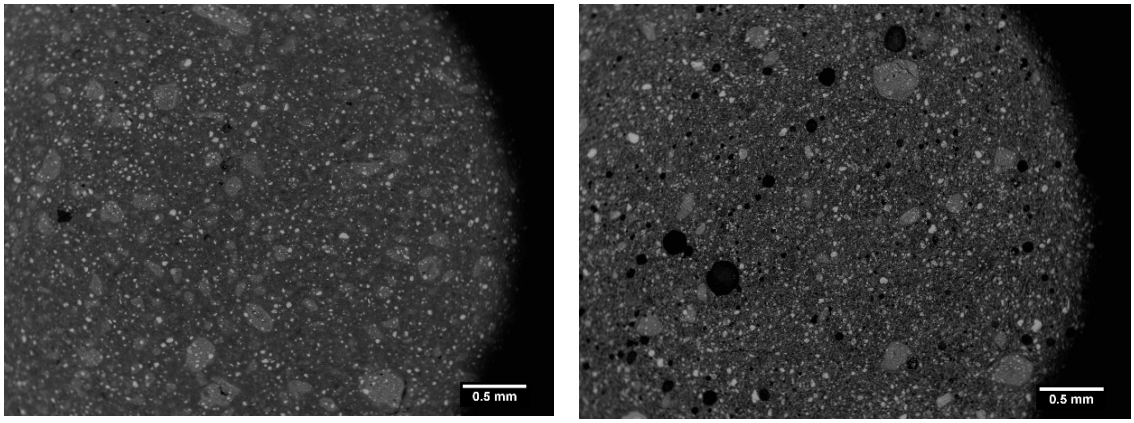

Figure 4-6 – The terrestrial gravity and microgravity sample on the left and right, respectively, show a significant difference in the amount of trapped air within the matrix.

Upon closer examination some differences in the microstructures are visible (Figure 4-7). The overall distribution of the hydration products is fairly spread out and equal throughout the matrix in the terrestrial sample. There is a dense ring of hydration products around the rim of the C_3A or the sight of a past grain of C_3A. However, when viewing the microgravity sample, it has dense clusters of hydration products with large concentrated pockets of porosity spread throughout the matrix. As will be discussed in more detail later, the porosity between the two samples is not as different as it may initially appear to with these larger pockets. The state of the hydration products around the C_3A is quite different for the two samples as the microgravity ones are exceptionally etched out with only a thin hydration shell covering the grain.

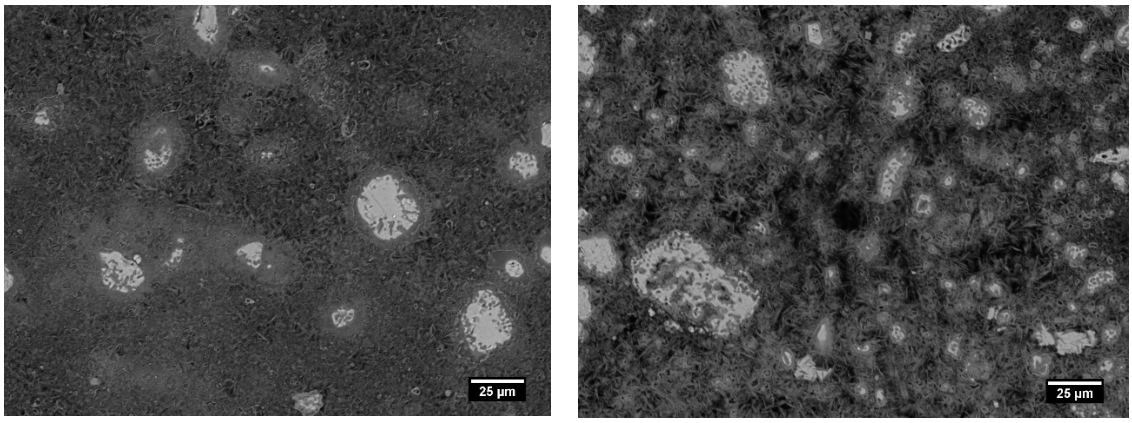

Figure 4-7 – Two images with a magnification of 500× for the samples that hydrated for 6 hours and 14 minutes, with terrestrial gravity being on the left and microgravity on the right.

4.1.3 Microstructural Differences at 22.97 Hours

The microstructural changes that occurred between 6 hours and 14 minutes to 22 hours and 58 minutes of hydration cannot be well characterized by the eye as the images appear similar. The C_3A grains within the terrestrial sample have started to become more etched in and filled with hydration products, but as can be seen in Figure 4-8 there are still grains that appear relatively intact with just a ring of hydration products surrounding the outside. In the microgravity sample, the vast majority of the C_3A grains are etched in and filled with hydration

products. Moreover, a dense rim or hydration products is typically not seen in the microgravity sample. This is likely due to diffusion controlling the transport phenomena of ions in the solution. There is still an apparent difference in the porosity distribution. Moreover, it is likely that the distribution of sulfur between the two systems is varied. Further work with a microprobe is needed to confirm such statements.

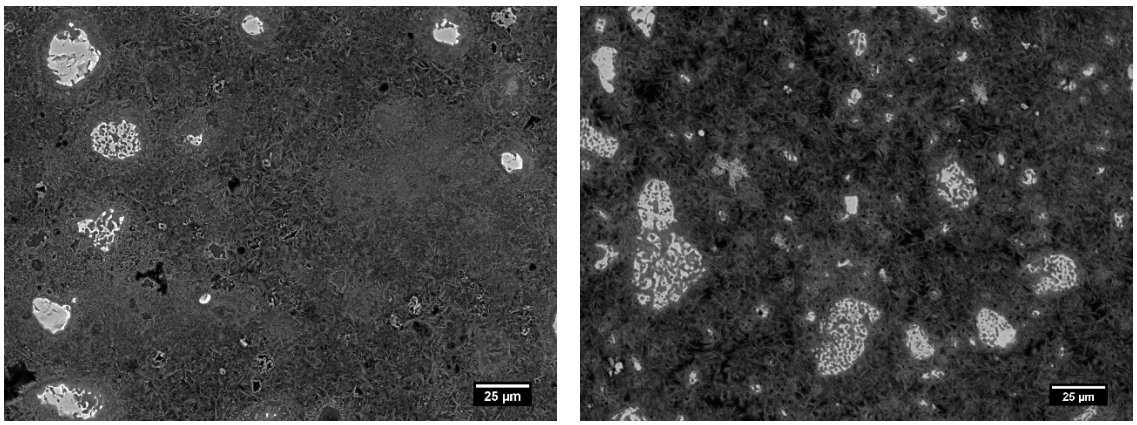

Figure 4-8 – A comparison of the polished samples for the terrestrial gravity and microgravity sample on the left and right, respectively.

4.1.4 Microstructural Differences for the Non-Flushed Specimen

The last set of samples that were analyzed within Series 1 were the ones that were not flushed with isopropanol up until they were ready to be analyzed. The microgravity samples were able to hydrate for approximately 32 days after mixing on the ISS before returning to Earth. However, hydration was not stopped until they were ready to be analyzed for fear of removing them from the pouch and exposing them to the atmosphere before analysis. As such, the microgravity sample hydrated for 32 days on the ISS which should account for the majority of the hydration in this fast reacting system, but any development past the 32 days occurred on Earth. As seen in the terrestrial gravity and microgravity sample there is minimal anhydrous C_3A visible. This is not surprising as they hydrated for 253 days before analysis. The microgravity sample still shows some larger pockets of porosity than are typically seen within the terrestrial

sample, but the overall microstructure at this point is similar to the eye for both samples (Figure 4-9).

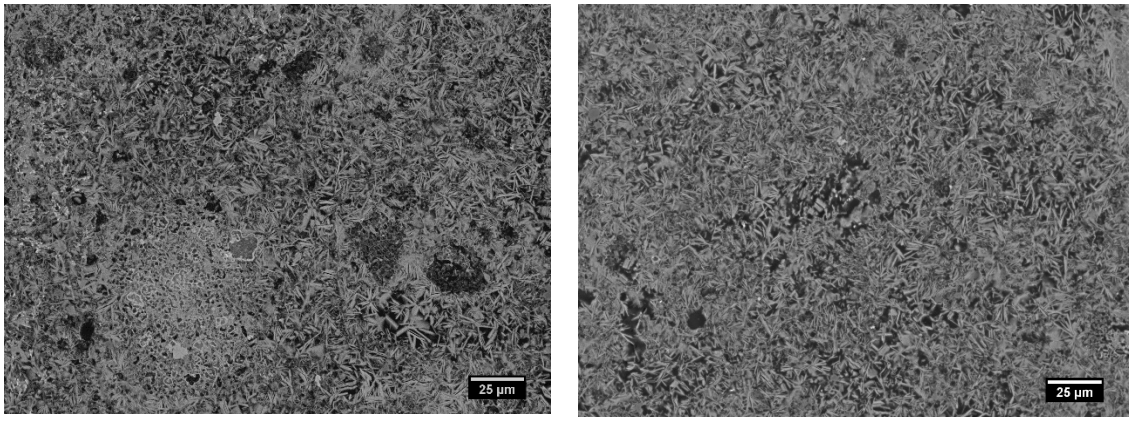

Figure 4-9 – Polished Series 1 samples that were not flushed with alcohol showing similar microstructures with terrestrial gravity and microgravity on the left and right, respectively.

4.1.5 Porosity Analysis for Series 1

The porosity of the microgravity and terrestrial gravity samples was calculated through image analysis for the samples that hydrated for 6 hours and 14 minutes, 22 hours and 58 minutes, and 253 days. The results of the analysis can be seen in Table 4-1. It can be seen for the terrestrial and microgravity sample the porosity remains relatively consistent from the three different times of analysis. When looking at the images this appears correct, as by the 6 hour and 14 minute mark a rather dense microstructure has developed. The average porosity of the microgravity sample is typically a couple of percent higher but when the standard deviation is considered with a hypothesis test, the results are not always statistically significant. The slight variation in porosity for each of the three times of the samples can be attributed to either sample prep, image acquisition, or the analysis.

In the previously published work a part of the MICS project a substantial difference in porosity was seen for the C_3S paste with the terrestrial and microgravity sample having porosities of 48.1 and 71.7 percent, respectively (Moraes Neves et al., 2019). The samples analyzed in the

C_3S work had a water to cement ratio of 2.0 as the goal was to provide ample space for crystals to grow and avoid restriction by the other hydration products. Since there is a lack of buoyancy forces within microgravity, the effect of bleeding is not seen in a manner that it is on Earth. Due to this reason, the effective water to cement ratios were not necessarily the same. However, MIP results from the study showed that the microgravity samples had a poorly distributed pore size distribution with a staggering amount around the 10 μm size. This result matches visually with the previously shown figures in this C_3A and Gypsum study as there is consistent large pockets of porosity seen in the microgravity sample.

Table 4-1 – Summary of the porosity measurements from analyzing twenty images per sample.

Sample	Average Porosity (%)	Standard Deviation (%)	Number of Images Required
Terrestrial – 6.23 Hours	20.39	3.2	11
Terrestrial – 22.97 Hours	18.66	2.93	11
Terrestrial – 253 Days	19.92	2.68	10
Microgravity – 6.23 Hours	22.29	3.88	14
Microgravity – 22.97 Hours	21.90	1.93	4
Microgravity – 253 Days	22.96	3.17	9

4.2 Series 2 Results and Discussion

4.2.1 Microstructural Differences at 2.47 Hours.

The Series 2 samples have 10% less gypsum than the Series 1 ones leading to a faster reaction. The difference in reaction rates for similar mixture designs has been researched and reported previously (Quennoz & Scrivener, 2012). The first set of samples within Series 2 hydrated for 2 hours and 28 minutes before being flushed with isopropanol. After viewing the fractured surfaces of the terrestrial sample, there were no remaining signs of gypsum within the sample. That is not to say gypsum doesn't exist, but it was not readily visible. The C_3A grains appeared well coated in hydration products and a dense matrix of hydration products had formed.

However, in the microgravity sample there were signs of where gypsum used to be present throughout the fractured surface.

The microstructure shown previously in Figure 4-2d for Series 1 had thin, rectangular clouds of hydration products present. An effort was made to locate any remaining intact pieces of gypsum in this Series 2 sample but none could be located as the only visible sign of any gypsum is an exoskeleton morphology filled with hydration products. After viewing such formations within the microgravity sample, the terrestrial sample was reimaged to find such features, but no such formations appeared to exist making this unique to the microgravity sample. An example of the typical terrestrial microstructure compared to the microgravity microstructure containing these areas of obvious places where gypsum used to be are seen in Figure 4-10. The terrestrial image is a lower magnification than the microgravity image to give the overall impression of the microstructure, where the microgravity one is meant to highlight the areas of past places of gypsum.

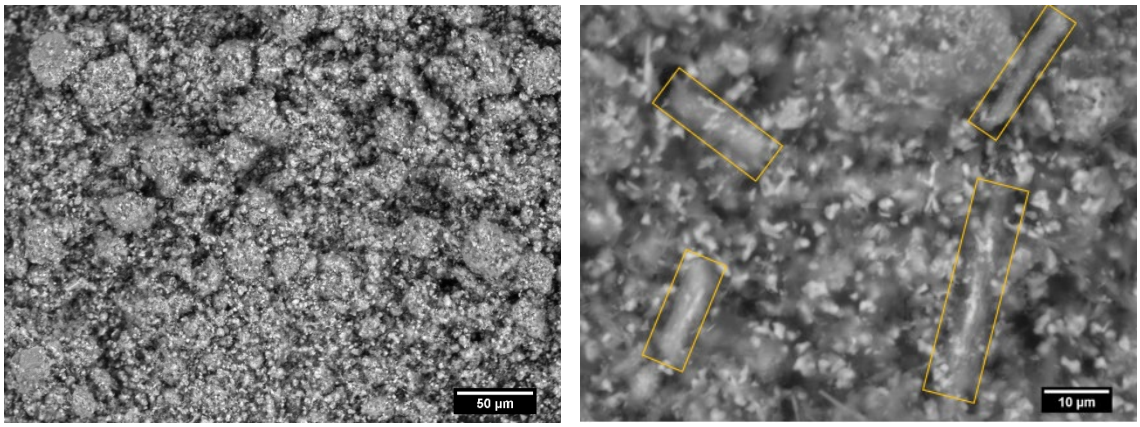

Figure 4-10 – The terrestrial sample on the left shows the general microstructure at the 2 hour and 28 minute mark. On the right, is the microgravity sample showing four areas of where gypsum used to be.

The structural integrity of the terrestrial gravity and microgravity samples in Series 2 were higher than the samples in Series 1 due to the quicker reaction kinetics with less gypsum. This made these samples easily polished for further examination with the SEM in combination

with energy dispersive X-ray spectroscopy (EDS). From a lower magnification, quite different microstructures are seen for the microgravity and terrestrial samples. The hydration products and overall microstructure in the terrestrial gravity sample appears uniformly distributed with minimal trapped air. As expected, the microgravity sample shows large cluster formations, trapped air, and a less dense microstructure.

There are multiple noticeable differences at a higher magnification, including the state of the C_3A grains, the amount of porosity and hydration products, and the visible spots of where gypsum used to exist. There is an apparent ring of hydration products coating the grains of C_3A in the terrestrial sample. This is similar to what was seen in Series 1 and reported in literature. The grains also show, for the most part, rather smooth perimeters at the boundary of the ring of hydration product and the C_3A grain. In comparison, there is a minimal ring around the C_3A grains within the microgravity sample. Furthermore, the surfaces of the C_3A grains are eroded and etched out. Very rarely is it seen that a larger grain has a smooth surface, as seen within the terrestrial sample. Upon closer examination of the grains, there is a substantial amount of hydration products growing off the edge of the grain. However, it is not to the point that a thick ring starts to form.

One may think that a heavily eroded C_3A grain may show signs of continued dissolution and therefore leading to the formation of an abundant amount of hydration products in comparing the terrestrial and microgravity samples. However, quite the opposite is true as the microstructure in the terrestrial sample is much more developed and showing a lot less porosity than the microgravity sample. Furthermore, there is an exoskeleton of the gypsum filled with a dense layer of hydration products. Figure 4-11 shows that this is no longer a piece of gypsum as the inside has hydration products growing in all directions and forming a thick matrix with a somewhat hollow core.

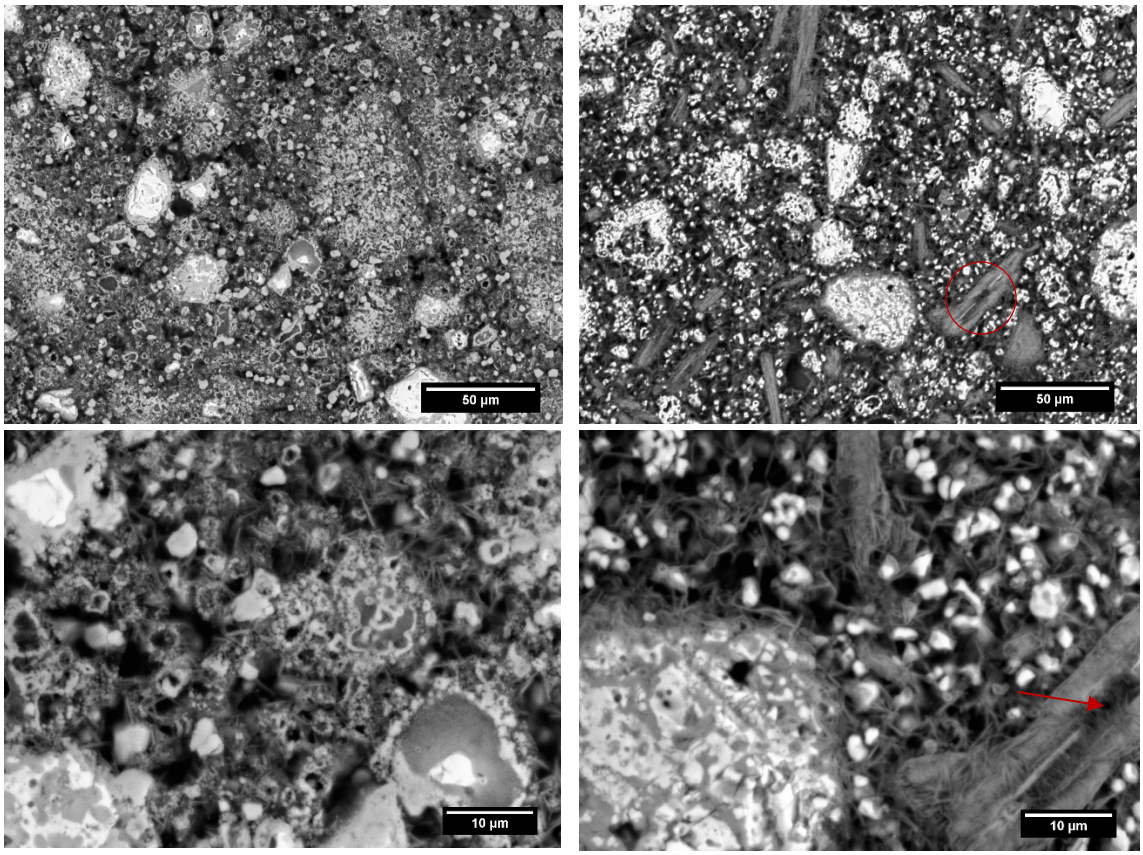

Figure 4-11 – The top left and right images show a comparison of the terrestrial and microgravity microstructures, respectively, at 2 hours and 28 minutes of hydration. The bottom show a higher magnification of the microstructure for the terrestrial (left) and microgravity (right) sample. The hollow core is noted with the circle and arrow.

To supplement the SEM image observations, 100 EDS points were taken from inside various exoskeletons of gypsum. The sulfur to calcium molar ratio was plotted vs the aluminum to calcium molar ratio for possible hydration products within the system, following a similar procedure to (Quennoz & Scrivener, 2012). The results of this analysis can be seen in Figure 4-12. If this was still intact gypsum, a molar ratio of 1:1 would be expected for the sulfur to calcium. Granted there is an interaction volume associated with the electrons that could be deeper than the area of interest so a perfect ratio would not be achieved. However, one would expect a ratio higher (closer to 1) than what is seen. Furthermore, the data reveals a substantial amount of aluminum within the system indicative of hydration products.

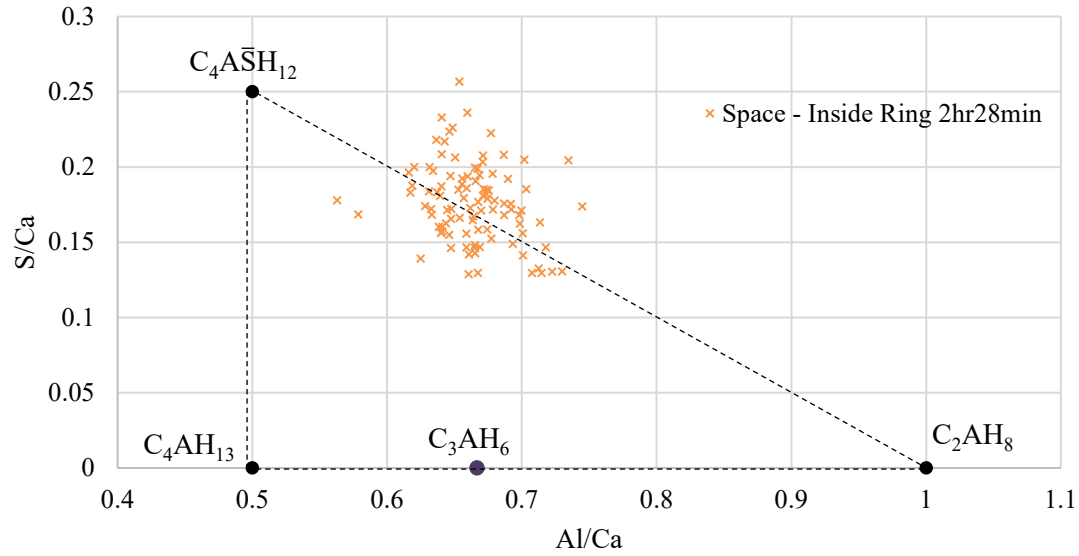

Figure 4-12 – EDS analysis of inside the gypsum exoskeleton at 2 hours and 28 minutes of hydration.

The reason for such dramatic differences at the 2 hour and 28 minute time within the terrestrial gravity and microgravity samples is related to the diffusion-controlled hydration process and minimized fluid convection. It has been shown that gypsum is used to hinder the rapid reaction of C_3A with water either by an adsorption phenomenon or ettringite growth, as previously discussed. There is also a substantial amount of heat released in these systems. The high heat release would promote fluid convection patterns and movement of ions within the terrestrial gravity system to allow it to reach a more homogenous state. The lack of fluid convection in microgravity in combination with diffusion-controlled growth and movement may lead to a mixture with areas lacking the necessary sulfate ions to stop the rapid dissolution of the C_3A allowing for a continued dissolution until a higher level of homogenous solution with respect to the sulfate is reached. The microgravity sample received additional assistance in transportation of ions via mixing for the first few minutes by the astronaut.

Also, it is important to remember that these systems start supersaturated with respect to calcium due to the lime water used. This may lead to a preferential dissolution of the alumina from the C_3A and sulfate from the gypsum. Due to the abundance of C_3A in this mixture, the calcium aluminate hydrates may form in the areas that do not contain sufficient gypsum, but the bigger part of the picture is the exoskeleton forming around the gypsum. For there still to be the shape of gypsum within the matrix means an amorphous ring formed around it which maintains the gypsums overall morphology (this ring becomes more apparent at later ages). With the system having a rapid release of alumina where the C_3A is not hindered as fast due to a lower gypsum content, this amorphous ring, similar to the AFm one on the C_3A reported in literature, can form. It is apparent that the concentration of ions around the gypsum is the favorable site for this amorphous ring to form at a lower gypsum content. This shows just how important gypsums role is in the dissolution of C_3A. If this amorphous ring formed very rapidly at the beginning blocking gypsums dissolution, it may be feasible that this sample may have reacted rapidly leading to a phenomenon like a flash set. However, it is impossible to say since these samples were not continually monitored for such observations on the ISS. The Series 1 system may contain just enough gypsum to where these effects seen in the microgravity Series 2 sample are minimized and this ring is not always formed.

In the Series 1 sample ettringite was seen growing on the surface of the gypsum and sometimes the growth was enough to give it a fuzzy appearance. However, the extra gypsum in the system may have supplied enough sulfate ions to hinder the dissolution of the C_3A and allow the gypsum to continue to dissolve in the system not allowing for a ring formation to surround it completely. This was not always the case in Series 1 as this exoskeleton formation was occasionally found but it was not overly abundant. While similar phenomenon can be seen in both, it is more prevalent in the Series 2 samples.

4.2.2 Microstructural Differences at 6.10 Hours

The next sample analyzed within Series 2 was flushed with alcohol at 6 hours and 6 minutes. The fractured surfaces of the samples were analyzed with the SEM to identify differences between the samples as well as changes from the 2 hour and 28 minute time of hydration. The terrestrial sample did not appear to change significantly from the fractured surface view, besides developing a denser matrix. However, the microgravity sample still showed the gypsum exoskeleton and the ring comprising the exoskeleton is readily apparent as the electron beam was able to penetrate it and show hydration products on the inside clearly. Figure 4-13 shows an example of one of the gypsum exoskeletons at this time. The clear view of the hydration products on the inside prompted the analysis of the polished sections as assumed the inside is becoming less dense making the features more visible or the outer ring is becoming thinner.

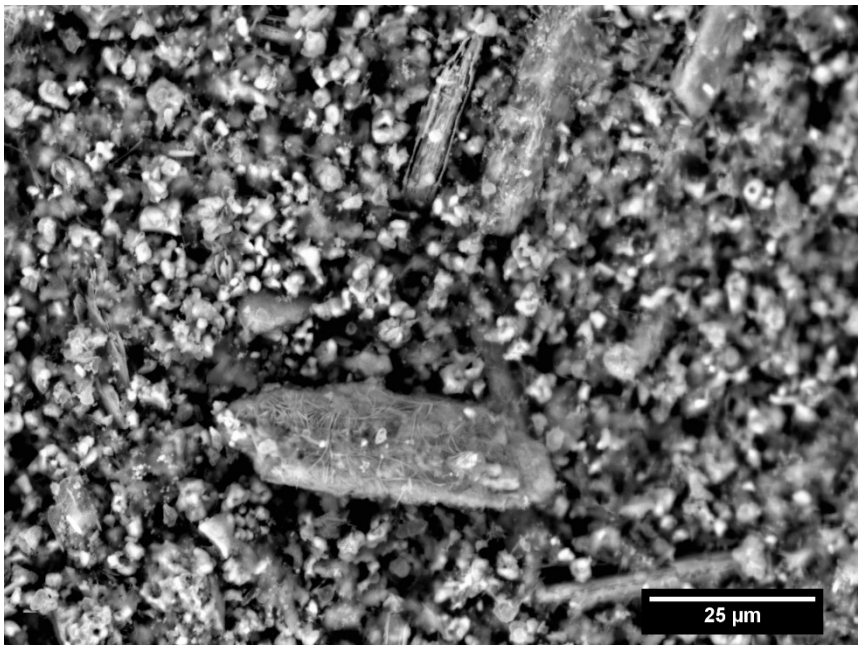

Figure 4 -13 – Just below the center of the image, a gypsum exoskeleton is seen with hydration products formed within the inside of the microgravity sample. At the top center of the image, there appears to be a similar formation that is more of a cross-sectional view with the outside ring apparent, a slight gap, and then hydration products on the inside.

The polished surfaces for the terrestrial and microgravity sample revealed interesting results in comparing to the previous flush time of 2 hours and 28 minutes. Some of the medium sized C_3A grains within the terrestrial sample have fully reacted leaving behind a hollow shell of hydrogarnet as seen in Figure 4-14. This is similar to what is seen in literature (Quennoz & Scrivener, 2012). The larger grains still show a substantial ring of hydration product around the outside edges, but some of the edges are becoming more eroded and less smooth than before. Hollow hydration rings are also visible for the microgravity sample for the smaller grains of C_3A, however, there are also thin and elongated hollow rings for the gypsum in the sample (Figure 4-14).

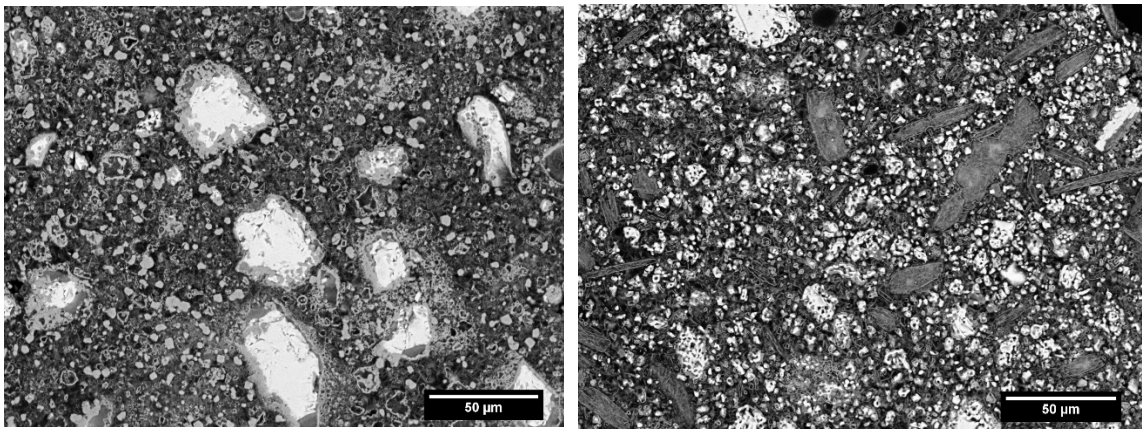

Figure 4-14 – A comparison of the polished surface microstructure at 6 hours and 6 minutes with the terrestrial sample on the left and the microgravity sample on the right.

The larger pieces of what used to be gypsum are still apparent, as seen earlier, but are becoming less dense now. There is now an obvious ring around the outside edge comprising the exoskeleton with the hydration products on the inside thinning out. The ring is imposing a barrier for the sulfate ions to diffuse through and react with the remaining C_3A. An EDS analysis similar to the one previously shown was conducted for the 6 hour and 6 minute flush times. 100 points were analyzed from the thin ring itself from various places throughout the microstructure and another 100 points from inside the ring analyzing the hydration products. Again, it should be

noted that there is an interaction volume associated with the electrons and the ring itself is quite small here. However, it does yield some interesting results that are seen in Figure 4-15. The inside of the ring itself is still centered around a similar aluminum to calcium ratio as before, with a slightly lower sulfur to calcium ratio as one would expect if the sulfate is diffusing out into the system. The other set of points on the graph are for the outside ring itself and show a shift down and to the right resulting in more aluminum and less sulfur as expected for an amorphous AFm phase. It is noted in literature that there is an miscibility gab between m-AFm and hydroxy-AFm so some combination of these at a sub-micron level may exist and influence the results (Matschei et al., 2007; Quennoz & Scrivener, 2012).

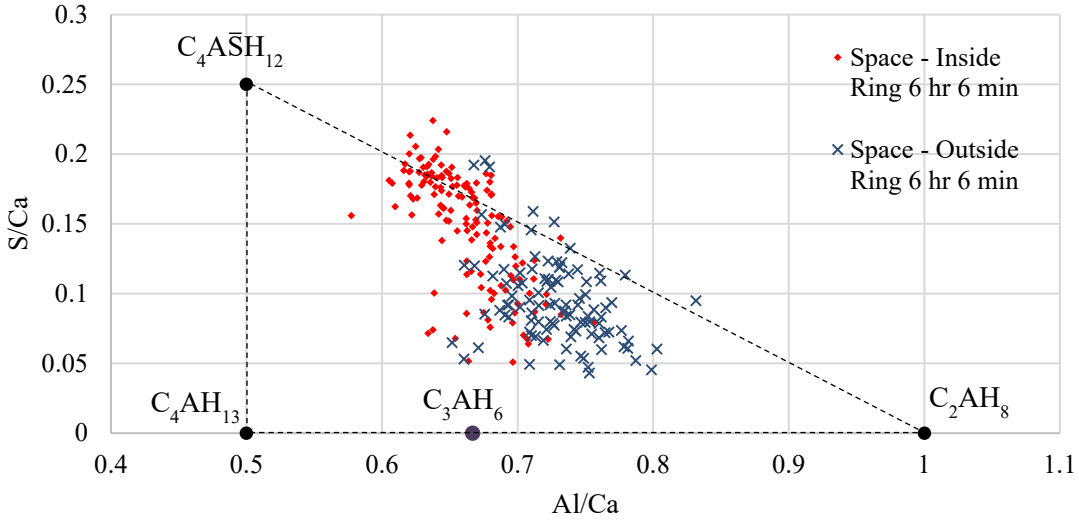

Figure 4-15 – An EDS analysis looking at the differences in the hydration products within and composing the exoskeleton of the gypsum.

4.2.3 Microstructural Differences at 23.35 Hours

The last set of samples flushed with alcohol were at 23 hours and 21 minutes. As previously done, fractured surfaces were viewed with the SEM to identify any unique differences. At this point, there were no unique changes that have not been presented already in previous

sections. The polished surfaces revealed results as expected for a microstructure that has hydrated for a slightly longer period of time. The C_3A in the microgravity sample was as eroded as before, however, a ring of hydration products is starting to densify around the outside of the grains now. Moreover, the exoskeletons for the gypsum still show signs of a ring with the middle continuing to hollow out and become less dense. An example of the two microstructures is shown in Figure 4-16.

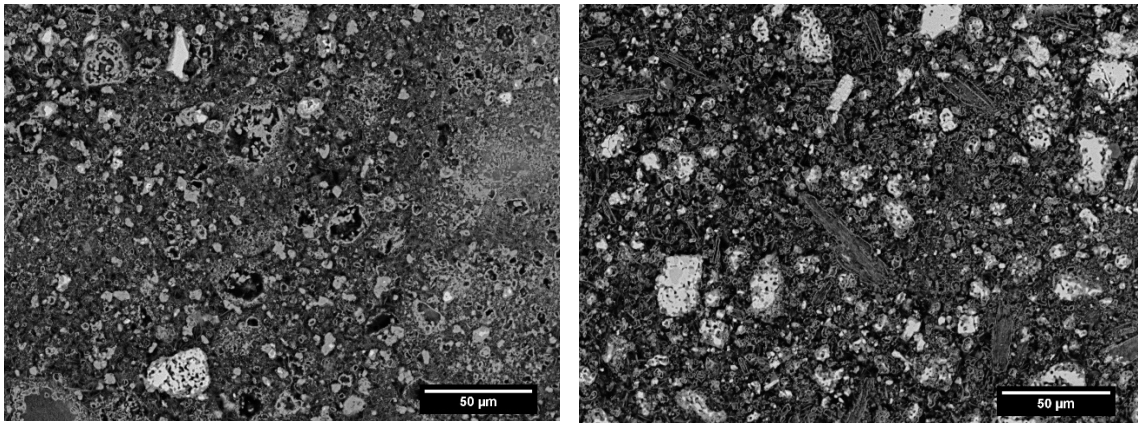

Figure 4-16 – A polished cross-section of the terrestrial and microgravity microstructure at 23 hours and 21 minutes, left and right, respectively.

An EDS analysis of the ring following the same procedure as described above was used to identify changes within the composition. Figure 4-17a shows an EDS analysis for the inside hydration products at the previously identified at 2 hours and 28 minutes, 6 hours and 6 minutes, and now at 23 hours and 21 minutes of hydration. A shift to less sulfur and more aluminum is seen for the hydration product within the ring furthering the idea that the sulfate is trapped within the ring and has to diffuse through the outer ring to react with the rest of the C_3A in the system. Another EDS analysis comparing the outside ring from the previous times can also be seen in Figure 4-17b. This reveals that there was little change in the composition of the ring as the majority of the data have stayed in the same place. There is a slight decrease in the overall sulfur

concentration, but this may be due to a slight interaction of electrons with the inside hydration products that are now starting to lose sulfur to the rest of the microstructural matrix.

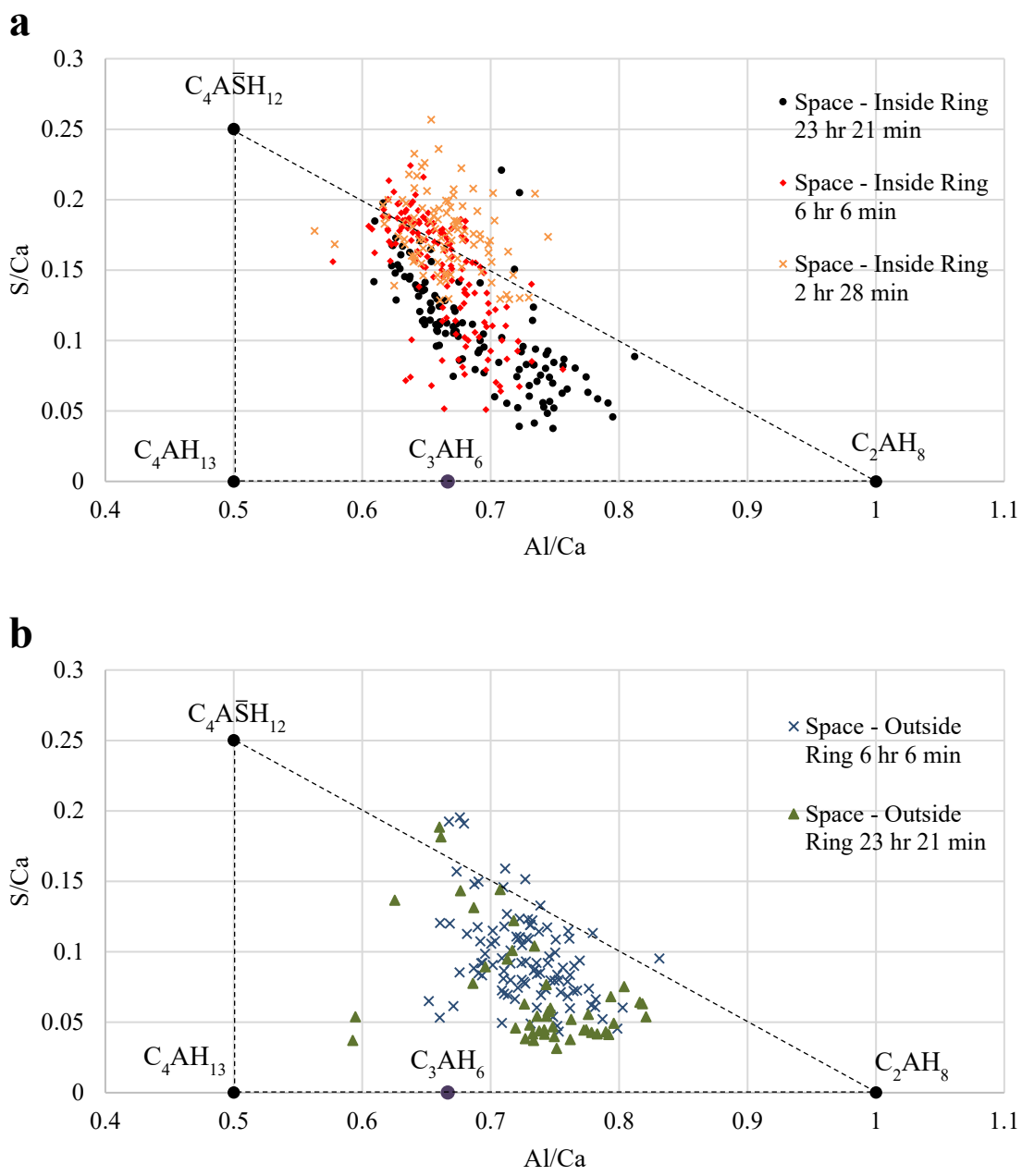

Figure 4-17 – EDS analysis of the microgravity microstructure. a) The top graph shows the hydration products within the exoskeleton ring and b) the bottom graph shows the ring itself.

4.2.4 Microstructural Differences for the Non-Flushed Specimen

The samples in series 2 that did not get flushed with alcohol until the time of analysis hydrated for a total of 385 days. Of that 385 days, the first 31 days of hydration occurred on the ISS. Like the no flush Series 1 samples, there is hydration that happened on Earth, but the majority of the microstructural development should have been in the microgravity environment. The area of interest, as seen in the previous sections, has been in the polished cross-sections of the samples. In comparing the terrestrial and microgravity sample, the microstructures have become substantially more similar than before. The microgravity sample reveals little to no signs of the amorphous gypsum exoskeleton anymore and a uniform looking matrix has formed. A visual comparison of the two samples can be seen in Figure 4-18. It should be noted that these microstructures are still likely to show differences in the concentrations of sulfur if microprobe work was done.

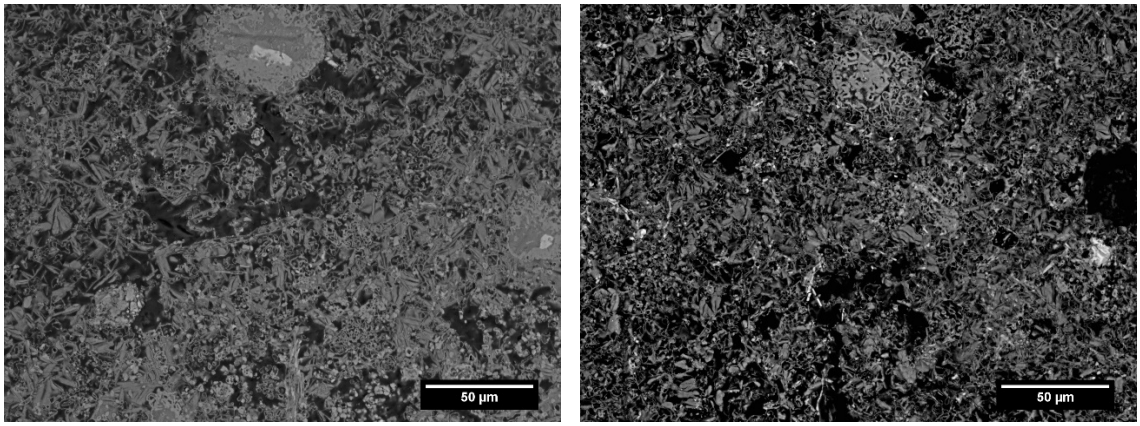

Figure 4-18 – A terrestrial sample seen on the left and the microgravity sample on the right revealing microstructures that have become more similar than seen previously.

Chapter 5

Conclusions and Future Work

5.1 Summary of Findings

The MICS project was pursued to better understand the complex hydration process of cement in the microgravity environment onboard the ISS. 120 samples with varying constituents were sent to the ISS to be mixed by astronauts. Isopropanol was used to arrest hydration of some of the samples at various times within the first 24 hours of hydration in order to track how the microstructure of the samples develop. In this thesis, the findings for two different series of samples containing C_3A and gypsum were presented. C_3A and gypsum make up a minor part of portland cement mixtures by volume but play a large role in the early age kinetics of the mixtures and set times. The primary means of analysis was with an SEM and the following conclusions were made:

- The samples that hydrated in the microgravity environment exhibit a nonuniform structure at early ages. This is characteristic of diffusion-controlled hydration process and minimized fluid convection.
- At later ages, both the microgravity and terrestrial gravity microstructures become more uniform than previously shown with the microgravity one containing more trapped air due to the lack of buoyancy. There are still differences within the microstructure, however further techniques, such as a microprobe, are needed to identify such features.
- The overall porosity seen in the Series 1 sample remains fairly constant at the three measured times, as verified through image analysis.
- The gypsum within the Series 1 sample is rather smooth for the terrestrial sample, matching literature well. However, in a microgravity environment the gypsum becomes

heavily striated showing characteristics of preferential dissolution and demand for hydration products in the vicinity.

- The initial gypsum content of the mixture (20% versus 10%) makes a substantial difference in the hydration process in microgravity as an amorphous ring abundantly forms around the Series 2 gypsum trapping in the sulfate within the system.
- At later ages in the Series 2 samples, the sulfate ions are starting to diffuse out of the amorphous ring and react with the C_3A.
- The C_3A in the microgravity sample shows signs of preferential dissolution as it becomes heavily errored around the edges.

5.2 Future Work

As NASA continues to work on the Artemis program, the need for a building material that is durable and resilient enough to withstand the harsh environments is a necessity. The goal to put humans back on the Moon in 2024 and have a sustained human presence by 2028 will only be possible if there is adequate infrastructure on the lunar surface. Concrete is viable material for such infrastructure given its ability to be formed in unique shapes, 3D printed, high resistance to extreme environments, and versatility in final design properties. While the ultimate goal is to manufacture a concrete using in-situ lunar resources to minimize the need to transport materials from Earth, the basic understanding of known Earth-based systems is a first and necessary step. The analysis of samples within the MICS project such as the C_3A and gypsum and C_3S mixtures are a fundamental step into understanding the effect that gravity has on these complex reactions. Knowledge of the pure components in portland cement will further the ability to explain the differences seen in the more complex mixtures such as OPC and the OPC with a lunar simulant.

The knowledge learned in these known and researched systems will help in designing a concrete using in-situ lunar materials.

To further the goal of designing a concrete building material for lunar infrastructure, the next step in the analysis is to research various samples at different gravity levels. As part of the MICS project, a second set of samples were sent to the ISS to be mixed and then placed within a centrifuge to mimic the gravity levels of the Moon, Mars, and a third data point ($7/10^{th}$ of Earth's gravity). These samples will allow for an understanding of what the cement solidification process will be theoretically like on the surface of these extraterrestrial bodies. With such an understanding and knowledge of these cementitious systems and the materials available on the surface of these extraterrestrial bodies, the ability of creating a concrete building material will prove to be even more viable.

Appendix A

Supplemental Studies

A.1 Clinostat Study

Several experimental methods have been developed in order to simulate a microgravity environment. Each method has significant disadvantages that make interpreting results of how microgravity influences the experiment difficult. One of the methods is a drop tower, where an object is dropped within the tower under vacuum allowing the object to appear weightless as it falls towards the bottom. Another technique is a parabolic flight where a plane has a steep trajectory upwards, cuts the engines, levels out, and starts to free fall before turning the engines back on and continuing the flight path. The shape of the flight resembles a bell curve. Both techniques are not perfect, as the time they provide for the experiments to be conducted in is less than a minute of simulated microgravity. The parabolic flight is also an expensive undertaking for research projects. However, an option that helps combat the time issue is the use of a clinostat.

A clinostat attempts to mimic microgravity by spinning a sample in the horizontal axis. If the sample is spun at the correct speed, the forces of gravity acting on the sample equal out. If the rotational speed is too slow, the sample will feel the force of gravity acting on it and if the speed is too fast, the sample becomes subjected to centrifugal forces (Akaiwa, Hardy, & Voorhees, 1991; Grugel, Kim, Woodward, & Wang, 1992; Yeckel, Patrick Doty, & Derby, 1999). It has been shown that a rotational speed of three rotations per minute is sufficient to achieve similar results to what is actually seen from experiments on the ISS in the microgravity environment. For that reason, a speed of three rpm was chosen for this experimental study.

The goal of this study was to see if the striations on the gypsum that are only abundantly seen in the microgravity Series 1 samples could be produced. Three different sample designs were used and spun for various times at the three-rpm speed as seen in Table A-1. The clinostat used for the study can be seen in Figure A-1. The system makes use of spinning 50 mL vials. For this study, a syringe needle was adhered to the middle of inside vial lid. The sample mixture was prepared and mounted on the tip of the needle using crystal bond. An example of a final mounted and prepared sample can be seen in Figure A-1. This setup allows for the sample to be spun around the center of the system helping cancel out the gravitational forces. The vial was filled all the way to the top with DI water and the lid for the vial, with the sample mounted, was screwed on and placed directly in the clinostat. After the time in the clinostat, the samples were removed and submerged within isopropanol for 15 minutes before examination with the SEM.

Table A-1 – Sample design and time spun on the clinostat

Sample	Spinning Time 1	Spinning Time 2	Spinning Time 3	Spinning Time 4
100% Gypsum	30 min	20 min	10 min	N/A
80% C_3A and 20% Gypsum	Static	5 min	15 min	N/A
50% C_3A and 50% Gypsum	Static	15 min	10 min	5 min

The results of achieving the striations were rather inconclusive as the gypsum never achieved the striations to the same degree that is seen in the microgravity samples. A possible reason for this could be due to how diluted the system is since the dissolution of gypsum is highly dependent upon the saturation of the system. For future work it would be advised to try to mimic the saturated, basic pH environment that would occur in the C_3A and gypsum systems within the first few minutes of mixing. However, the gypsum did show signs of dissolution that is not the typical layer by layer process that is typically seen. This may suggest that the striations could be achieved if the solution chemistry was altered.

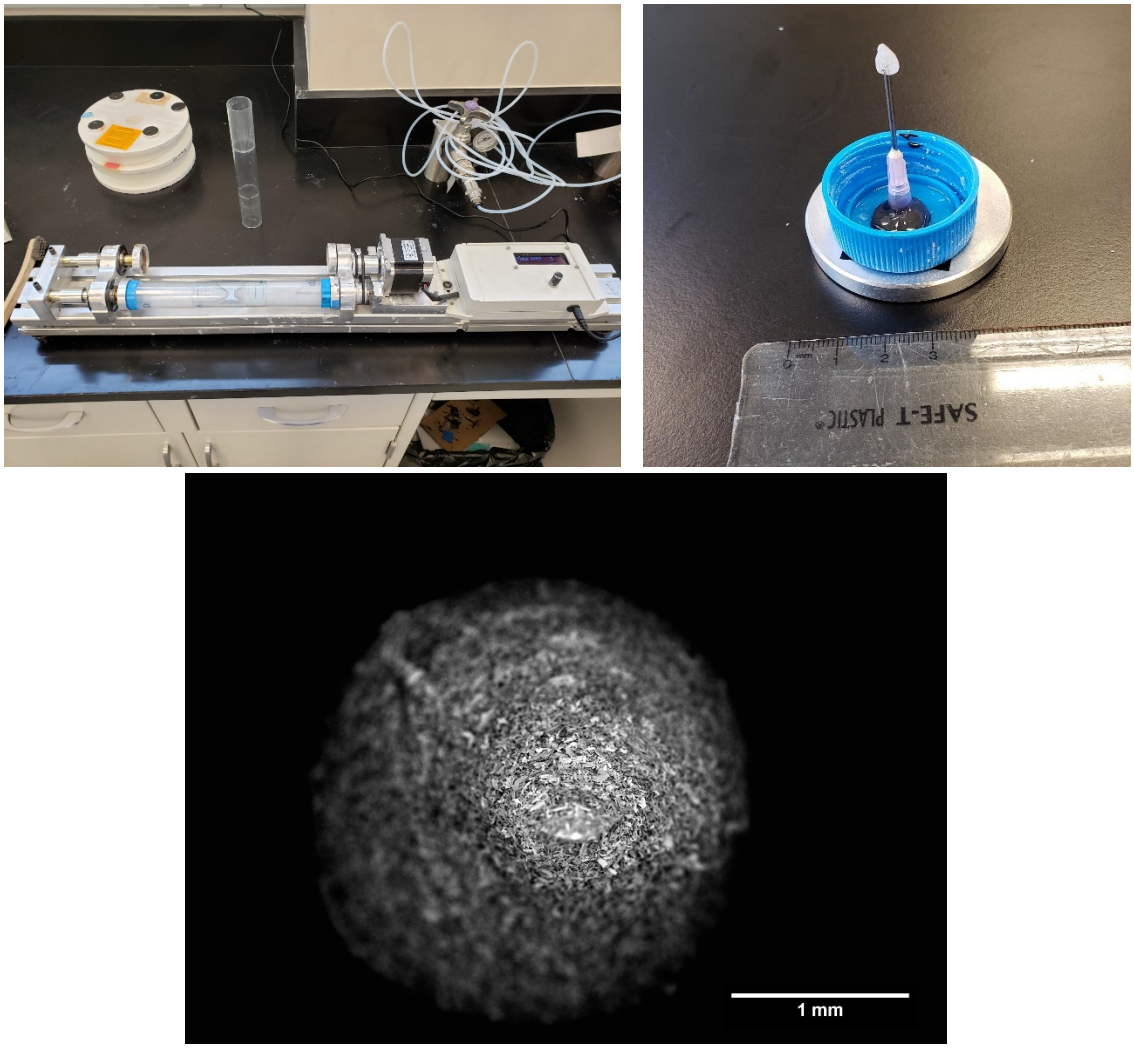

Figure A-1 – On the top left is the clinostat machine. Four of the 50-mL vials can be supported at one time. On the top right is a prepared sample with the powder on the crystal bond on the needle tip. The bottom image is an SEM image looking down on the needle before the test.

The 100% gypsum samples were a starting point in the clinostat study and the first two spinning times were too long as most of the gypsum was no longer present on the needle. There was still a significant amount of gypsum available within the sample that was spun for 10 minutes. A picture of the state of the gypsum in a static state from 10-minute exposure to the water in the vial can be seen in Figure A-2. A comparison to a piece of gypsum from the clinostat at the 10-minute mark can also be seen in Figure A-2.

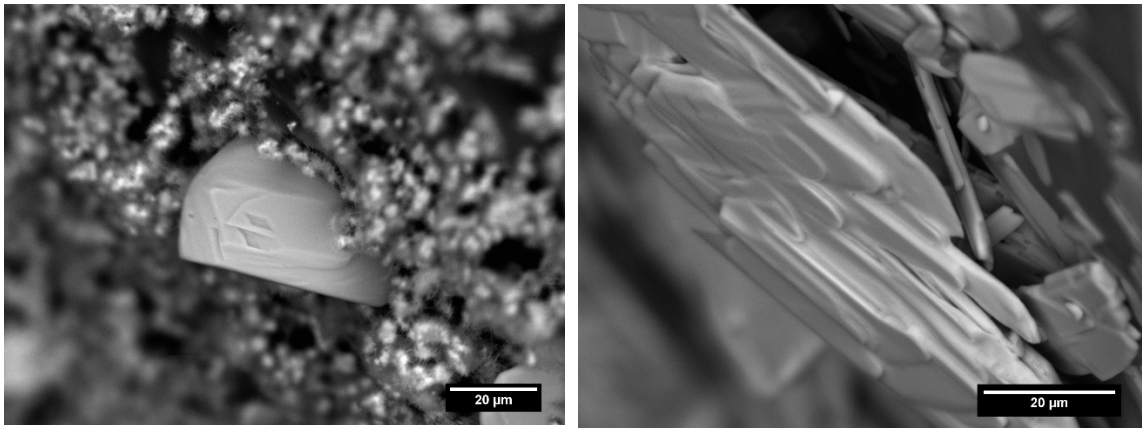

Figure A-2 – On the left and right are pieces of gypsum that were in the static state and spun at 3 rpm in the clinostat, respectively.

Besides the state of the gypsum, substantial ettringite growth on the C_3A grains can be seen. An observation that is unique to the samples that were spun in the clinostat is a cluster formation of hydration products. This is a similar idea to the AFm clusters that are seen in the microgravity samples in areas of decomposing gypsum. It may be speculated that some of these clusters in the clinostat study could be an area of a past piece of gypsum but there is no strong evidence of this like there was in the microgravity samples. A comparison of the microstructure from the static state for 5 minutes and spun for 5 minutes within the clinostat can be seen in Figure A-3.

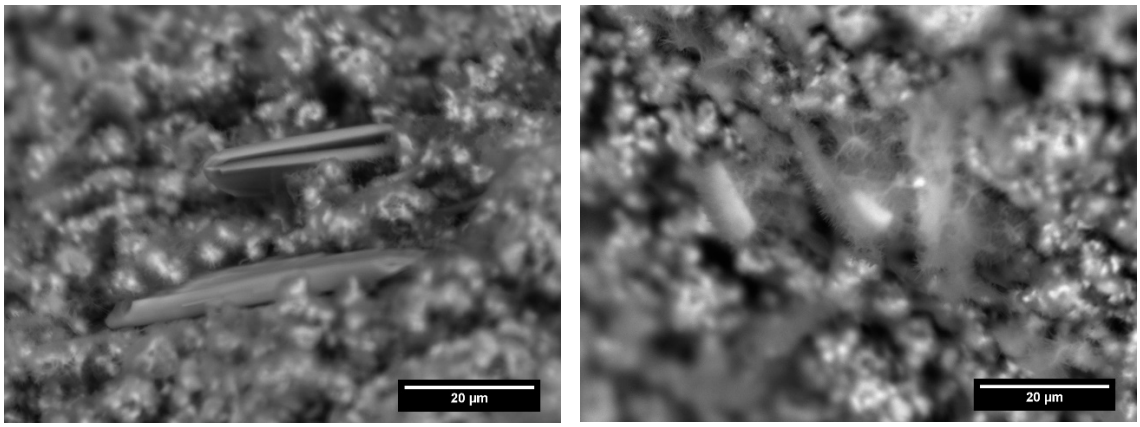

Figure A-3 –. The image on the left is from the static condition for 5 minutes. On the right is a formation of a cluster of ettringite from hydration within the clinostat for 5 minutes

A.2 Prolonged Alcohol Exposure Study

A significant number of samples within the MICS study were flushed with isopropyl alcohol at 3 hours, 7 hours, and 24 hours after mixing. The presence of alcohol allows for the hydration of the cement paste to be stopped, by effectively removing the water from the system so it can no longer react with the cement. This is possible as isopropanol and water are completely miscible. This project setup was desired to identify how the microstructures develop as a function of time and the technique is heavily used within cementitious materials research. However, the samples that are subjected to isopropanol are typically only left in the alcohol for a week and then removed for analysis.

The samples within the MICS experiment were left in the alcohol until they were ready to be analyzed in order to prevent them from unwanted exposure to the atmosphere. There has been little work done on whether subjecting cementitious materials to prolonged alcohol exposure is detrimental to the microstructure. A question was raised to whether the prolonged exposure of alcohol had anything to do with the morphological differences seen in the gypsum. Samples of anhydrous C_3A and gypsum were placed in isopropanol alcohol to be analyzed after 1 week, 1 month, 3 months, 6 months, and 1 year. SEM images were taken before alcohol exposure to set a baseline morphology and can be seen in Figure A-4. To date the samples have been analyzed with the SEM at 1 week and 1 month; the results can be seen in Figure A-5 and Figure A-6, respectively. Thus far the samples have showed no signs of any morphological differences from the alcohol exposure.

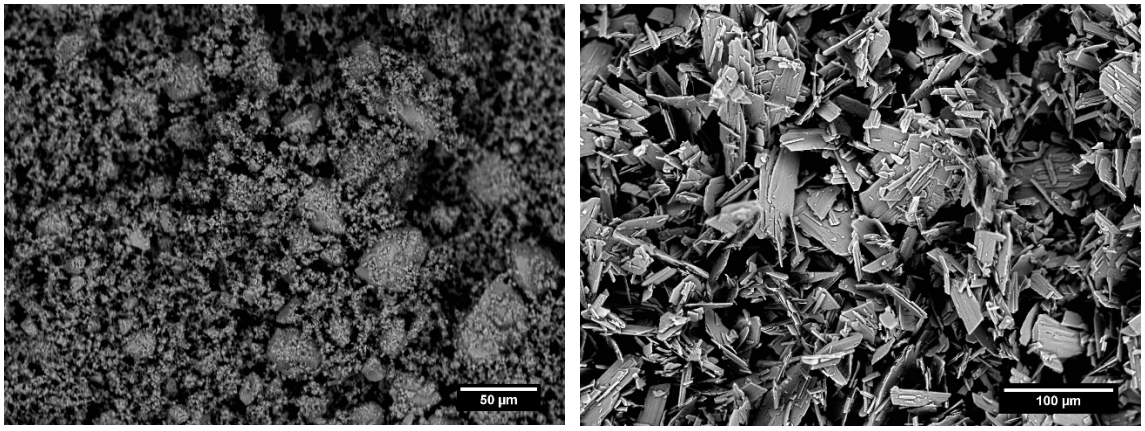

Figure A-4 – C_3A and gypsum on the left and right, respectively, before alcohol exposure.

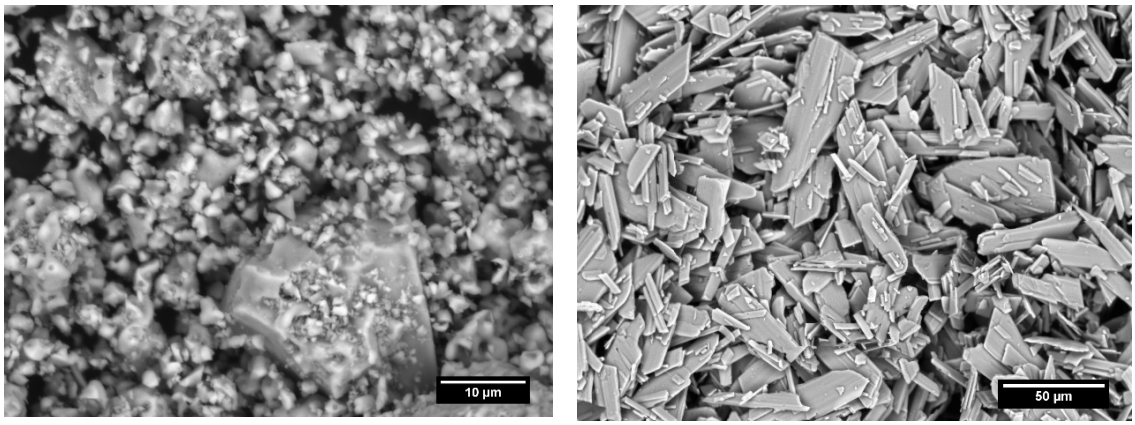

Figure A-5 – C_3A and gypsum on the left and right, respectively, after one week of exposure to isopropanol.

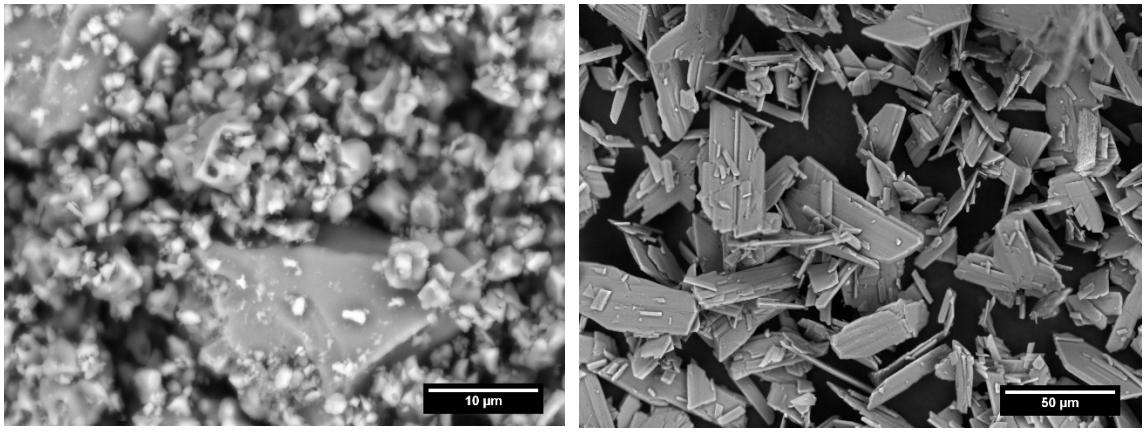

Figure A-6 – C_3A and gypsum on the left and right, respectively, after one month of exposure to isopropanol.

References

Akaiwa, N., Hardy, S. C., & Voorhees, P. W. (1991). The effects of convection on Ostwald ripening in solid-liquid mixtures. *Acta Metallurgica Et Materialia*, *39*(11), 2931–2942. https://doi.org/10.1016/0956-7151(91)90109-E

Baquerizo, L. G., Matschei, T., & Scrivener, K. L. (2016). Cement and Concrete Research Impact of water activity on the stability of ettringite. *Cement and Concrete Research*, *79*, 31–44. https://doi.org/10.1016/j.cemconres.2015.07.008

Baquerizo, L. G., Matschei, T., Scrivener, K. L., Saeidpour, M., & Wadsö, L. (2015). Hydration states of AFm cement phases. *Cement and Concrete Research*, *73*, 143–157. https://doi.org/10.1016/j.cemconres.2015.02.011

Black, L., Breen, C., Yarwood, J., Deng, C. S., Phipps, J., & Maitland, G. (2006). Hydration of tricalcium aluminate (C3A) in the presence and absence of gypsum - Studied by Raman spectroscopy and X-ray diffraction. *Journal of Materials Chemistry*, *16*(13), 1263–1272. https://doi.org/10.1039/b509904h

Bosbach, D., & Rammensee, W. (1994). In situ investigation of growth and dissolution on the (010) surface of gypsum by Scanning Force Microscopy. *Geochimica et Cosmochimica Acta*, *58*(2), 843–849. https://doi.org/10.1016/0016-7037(94)90509-6

Capabilities & Services. (2019). Retrieved from https://www.spacex.com/about/capabilities

Collepardi, M., Baldini, G., Pauri, M., & Corradi, M. (1979). Retardation of Tricalcium Aluminate Hydration by Calcium Sulfate. *Journal of the American Ceramic Society*, *62*(1–2), 33–35. https://doi.org/10.1111/j.1151-2916.1979.tb18800.x

Dunbar, B. (2019). Explore Moon to Mars. Retrieved from https://www.nasa.gov/specials/moon2mars/#artemis

Fan, C., & Teng, H. H. (2007). Surface behavior of gypsum during dissolution. *Chemical*

Geology, *245*(3–4), 242–253. https://doi.org/10.1016/j.chemgeo.2007.08.007

Feldman, R. F., & Ramachandran, V. S. (1966). The influence of CaSO 4 .2H 2 O upon the hydration character of 3CaO.Al 2 O 3. *Magazine of Concrete Research*, *18*(57), 185–196. https://doi.org/10.1680/macr.1966.18.57.185

Futron Corporation. (2002). Space Transportation Costs: Trends in Price Per Pound to Orbit 1990-2000. *Whitepaper*.

Geng, G., Myers, R. J., Yu, Y. S., Shapiro, D. A., Winarski, R., Levitz, P. E., … Monteiro, P. J. M. (2018). Synchrotron X-ray nanotomographic and spectromicroscopic study of the tricalcium aluminate hydration in the presence of gypsum. *Cement and Concrete Research*, *111*(June), 130–137. https://doi.org/10.1016/j.cemconres.2018.06.002

Grugel, R. N., Kim, S., Woodward, T., & Wang, T. G. (1992). The effect of axial crucible rotation on microstructural uniformity during horizontal directional solidification. *Journal of Crystal Growth*, *121*(4), 599–607. https://doi.org/10.1016/0022-0248(92)90567-3

Joseph, S., Skibsted, J., & Cizer, Ö. (2019). A quantitative study of the C3A hydration. *Cement and Concrete Research*, *115*(June 2018), 145–159. https://doi.org/10.1016/j.cemconres.2018.10.017

Lasaga, A. C., & Luttge, A. (2001). Variation of crystal dissolution rate based on a dissolution stepwave model. *Science*, *291*(5512), 2400–2404. https://doi.org/10.1126/science.1058173

Lei, L., Meier, M. R., Rinkenburger, A., Baicun, Z., Lefeng, F., & Plank, J. (2016). Early hydration of portland cement admixed with polycarboxylates studied under terrestric and microgravity conditions. *Journal of Advanced Concrete Technology*, *14*(3), 102–107. https://doi.org/10.3151/jact.14.102

Loff, S. (2019). The Apollo Missions. Retrieved September 3, 2019, from https://www.nasa.gov/mission_pages/apollo/missions/index.html

Matschei, T., Lothenbach, B., & Glasser, F. P. (2007). The AFm phase in Portland cement.

Cement and Concrete Research, *37*(2), 118–130. https://doi.org/10.1016/j.cemconres.2006.10.010

McPherson, A., Malkin, A. J., Kuznetsov, Y. G., Koszelak, S., Wells, M., Jenkins, G., … Lawson, G. (1999). The effects of microgravity on protein crystallization: Evidence for concentration gradients around growing crystals. *Journal of Crystal Growth*, *196*(2–4), 572–586. https://doi.org/10.1016/S0022-0248(98)00853-7

Mehta, P. K. (1976). Scanning electron micrographic studies of ettringite formation. *Cement and Concrete Research*, *6*(2), 169–182. https://doi.org/10.1016/0008-8846(76)90115-0

Mehta, P. K., & Monteiro, P. J. M. (2006). *Concrete Microstructure, Properties, and Materials*. *The British Journal of Psychiatry* (Third, Vol. 112). The McGraw-Hill Companies, Inc. https://doi.org/10.1192/bjp.112.483.211-a

Meier, M. R., & Plank, J. (2016). Crystal growth of [Ca3Al(OH)6.12H2O]2.(SO4)3.2H2O (ettringite) under microgravity: On the impact of anionicity of polycarboxylate comb polymers. *Journal of Crystal Growth*, *446*, 92–102. https://doi.org/10.1016/j.jcrysgro.2016.04.049

Meier, M. R., Sarigaphuti, M., Sainamthip, P., & Plank, J. (2015). Early hydration of Portland cement studied under microgravity conditions. *Construction and Building Materials*, *93*, 877–883. https://doi.org/10.1016/j.conbuildmat.2015.05.074

Minard, H., Garrault, S., Regnaud, L., & Nonat, A. (2007). Mechanisms and parameters controlling the tricalcium aluminate reactivity in the presence of gypsum. *Cement and Concrete Research*, *37*, 1418–1426. https://doi.org/10.1016/j.cemconres.2007.06.001

Moraes Neves, J., Collins, P. J., Wilkerson, R. P., Grugel, R. N., & Radlińska, A. (2019). Microgravity Effect on Microstructural Development of Tri-calcium Silicate (C3S) Paste. *Frontiers in Materials*, *6*(April), 1–12. https://doi.org/10.3389/fmats.2019.00083

Myers, R. J., Geng, G., Li, J., Rodríguez, E. D., Ha, J., Kidkhunthod, P., … Monteiro, P. J. M.

(2016). Role of adsorption phenomena in cubic tricalcium aluminate dissolution. *Langmuir*, *33*(1), 45–55. https://doi.org/10.1021/acs.langmuir.6b03474

NASA. (2018). NASA Image: ISS056E073250. Washington D.C.: NASA. Retrieved from https://www.nasa.gov/mission_pages/station/research/experiments/explorer/Investigation.html?#id=7658

Pachon-Rodriguez, E. A., & Colombani, J. (2013). Pure dissolution kinetics of anhydrite and gypsum in inhibiting aqueous salt solutions. *AIChE Journal*, *59*(5), 1622–1626. https://doi.org/10.1002/aic.13922

Planetary Science Communications Team. (2019a). Earth's Moon: In Depth. Retrieved September 3, 2019, from https://solarsystem.nasa.gov/moons/earths-moon/in-depth/

Planetary Science Communications Team. (2019b). Mars: In Depth. Retrieved September 3, 2019, from https://solarsystem.nasa.gov/planets/mars/in-depth/

Pommersheim, J., & Chang, J. (1986). Kinetics of hydration of tricalcium aluminate. *Cement and Concrete Research*, *16*(3), 440–450. https://doi.org/10.1016/0008-8846(86)90120-1

Pommersheim, J., & Chang, J. (1988). Kinetics of Hydration of Tricalcium Aluminate in the Presence of Gypsum. *Cement and Concrete Research*, *18*(6), 911–922.

Quennoz, A., & Scrivener, K. L. (2012). Hydration of C3A – gypsum systems. *Cement and Concrete Research*, *42*(7), 1032–1041. https://doi.org/10.1016/j.cemconres.2012.04.005

Scrivener, K. L., Juilland, P., & Monteiro, P. J. M. (2015). Advances in understanding hydration of Portland cement. *Cement and Concrete Research*, *78*, 38–56. https://doi.org/10.1016/j.cemconres.2015.05.025

Seligmann, P., & Greening, N. R. (1964). Studies of early hydration reactions of portland cement by X-ray diffraction. *Highway Research Record*, *62*, 80–105.

Skalny, J., & Tardos, M. E. (1977). Retardation of Tricalcium Aluminate Hydration by Sulfates. *Journal of the American Ceramic Society*, *60*(3–4), 174–175. https://doi.org/10.1111/j.1151-

2916.1977.tb15503.x

Stein, H. N. (1962). Some characteristics of the hydration of 3CaO.Al2O3 in the presence of CaSO4.2 H2O. *Recueil Des Travaux Chimiques Des Pays-Bas*, *81*(10), 881–889. https://doi.org/10.1002/recl.19620811008

Taylor, H. F. W. (1990). Cement Chemistry (2nd ed., p. 35). London: Academic Press.

Vickers, J., Tate, L., Chandler, F., Coppens, C., Dube, M., Johnson, S., … Scottie, S. (2015). NASA Technology Roadmaps and Manufacturing. *NASA Technology Roadmaps*, 15–24.

Wong, H. S., Head, M. K., & Buenfeld, N. R. (2006). Pore segmentation of cement-based materials from backscattered electron images. *Cement and Concrete Research*, *36*(6), 1083–1090. https://doi.org/10.1016/j.cemconres.2005.10.006

Yeckel, A., Patrick Doty, F., & Derby, J. J. (1999). Effect of steady crucible rotation on segregation in high-pressure vertical Bridgman growth of cadmium zinc telluride. *Journal of Crystal Growth*, *203*(1), 87–102. https://doi.org/10.1016/S0022-0248(99)00065-2

Zareeipolgardani, B., Piednoir, A., & Colombani, J. (2017). Gypsum Dissolution Rate from Atomic Step Kinetics. *Journal of Physical Chemistry C*, *121*(17), 9325–9330. https://doi.org/10.1021/acs.jpcc.7b00612

Zhao, H., & Darwin, D. (1992). Quantitative backscattered electron analysis of cement paste. *Cement and Concrete Research*, *22*(4), 695–706. https://doi.org/10.1016/0008-8846(92)90022-N